Quantification of trace element atmospheric deposition fluxes to the Atlantic Ocean (>40°N; GEOVIDE, GEOTRACES GA01) during spring 2014

Shelley Rachel U. [1, *], Roca-Marti Montserrat [2, 3], Castrillejo Maxi [2, 3], Masque Pere [2, 3, 4, 5],
Landing William M. [6], Planquette Helene [1], Sarthou Geraldine [1]

[1] Inst Univ Europeen La Mer, CNRS UBO IRD IFREMER, Lab Sci Environm Marin, UMR LEMAR 6539, Technopole Brest Iroise, F-29280 Plouzane, France.
[2] Univ Autonoma Barcelona, Dept Fis, Barcelona 08193, Spain.
[3] Univ Autonoma Barcelona, Inst Ciencia & Tecnol & Ambientals, Barcelona 08193, Spain.
[4] Edith Cowan Univ, Sch Nat Sci, 270 Joondalup Dr, Joondalup, WA 6027, Australia.
[5] Univ Western Australia, Oceans Inst & Sch Phys, 35 Stirling Highway, Crawley, WA 6009, Australia.
[6] Florida State Univ, Sch Earth Ocean & Atmospher Sci, 117 N Woodward Ave, Tallahassee, FL 32306 USA.

* Corresponding author : Rachel U. Shelley, email address : rachel.shelley@univ-brest.fr

Abstract :

Atmospheric deposition is an important input route of trace elements (TEs) to the global ocean. As atmospheric inputs impact phytoplankton community health and dynamics, atmospheric TE fluxes, and in particular atmospheric iron fluxes, are a key component of marine biogeochemical models. Trace element concentrations were determined in dry (aerosols) and wet (precipitation) deposition samples from the North Atlantic, north of 40 °N, during the GEOVIDE cruise (GEOTRACES cruise GA01) in May/June 2014. Atmospheric aerosol loading in the study region was low (~ 2–500 ng m-3) throughout the cruise, as inferred from the very low aerosol Ti concentrations determined (0.0084–1.9 ng m-3). Wet deposition appeared to be of roughly equal or greater importance than dry deposition to the total depositional flux of TEs, which is consistent with other regions of the Atlantic Ocean outside of the influence of the Saharan plume.

It can be challenging to convert aerosol chemical composition data into reliable flux estimates, due to the uncertainties associated with the parameterisation of dry deposition velocity, and precipitation rate.

Therefore, the goal of this study was to compare TE flux estimates derived from two different techniques: (1) the traditional approach of summed wet and dry deposition TE fluxes, using concentration data, precipitation rates, and dry deposition velocities and, (2) using the inventory of the cosmogenic radioisotope beryllium-7 (7Be) in the upper ocean as a proxy for atmospheric deposition. These two approaches yielded TE flux estimates that were in excellent agreement (within one standard deviation) for about half of the TEs under investigation. However, for the remaining TEs differences between the flux estimates ranged from two to forty times, with the traditional approach generally being the higher of the

two estimates. Therefore, factors that may contribute to this variation, such as differences in the timescale of integration and selection of representative deposition velocities and precipitation rates, are discussed. Our results suggest that the 7Be approach continues to show promise in this application, particularly in regions where precipitation samples cannot be routinely collected.

Highlights

► Atmospheric deposition of trace elements was low north of 40°N in May/June 2014. ► The radioisotope ^{7}Be was used as a proxy for atmospheric deposition. ► Flux estimates from (1) wet plus dry deposition; (2) the seawater inventory of ^{7}Be. ► Similar flux values for some elements, but large differences for others.

Keywords : Atmospheric deposition fluxes, Trace elements, Be-7, Atlantic Ocean, GEOTRACES

INTRODUCTION

Atmospheric deposition is an important input route of trace elements (TEs) to the global ocean, and can be the principal input in some open ocean regions (Jickells et al., 2005). Atmospheric deposition

59   is delivered to the surface ocean via wet (rain, fog, snow) and dry deposition (dust, soil, ash). It is

60   important to quantify the total atmospheric deposition fluxes of TEs (both essential and potentially

61   deleterious) to the surface ocean as atmospheric inputs impact phytoplankton community health and

62   dynamics. Thus, in this way, atmospheric TE inputs may be linked to the global C and N cycles, key

63   players in the global climate system (Morel and Price, 2003; Sunda, 2012). Yet many areas of the global

64   ocean are limited, or co-limited by TE availability (Saito et al., 2008; Moore et al., 2013). Understanding

65   the processes that govern TE supply and availability are key for gaining a mechanistic understanding of

66   the biological carbon pump. However, atmospheric deposition remains poorly constrained, largely due

67   to the difficulties associated with quantifying fluxes (Law et al., 2013).

68   The magnitude of aerosol input to the atmosphere from dust producing regions is a function of

69   wind speed and precipitation in those regions. The magnitude of aerosol deposition downwind from

70   aerosol source regions is a function of atmospheric loading, particle size and type, wind speed, humidity

71   and precipitation in the receiving areas (Moulin et al., 1997). Even in the North Atlantic Ocean, which

72   receives the largest inputs due to its proximity to the Sahara Desert (~40% of annual global dust

73   deposition; Jickells et al., 2005), aerosol deposition is not uniformly distributed. The Sahara outflow

74   transports vast quantities of mineral dust (~1 x 10^{12} tonnes a year; d'Almeida, 1986) over the Atlantic

75   Ocean, as far as the Americas, at altitudes above the marine boundary layer (MBL; ~500-6000 m;

76   Prospero and Carlson, 1972), approximately over the latitudinal band 5-30°N. To the south, the Saharan

77   dust plume is largely constrained by the seasonally-migrating intertropical convergence zone (ITCZ; ~5-

78   10°N) (Prospero and Carlson, 1972; Doherty et al., 2012; Schlosser et al., 2013), and to the north by the

79   northern extent of the trade winds (~30°N). North of 30°N, a steep declining gradient in atmospheric

80   aerosol loading, as determined by metrics such as aerosol optical depth (AOD; e.g.

81   http://aeronet.gsfc.nasa.gov), is observed due to a combination of increasing distance from North

82   African dust source regions and large-scale atmospheric circulation. As a result, other aerosol sources

83   (Europe, North America, sea salt and, occasionally, volcanoes) become relatively more important in the

84   north of this ocean basin. Thus, several aerosol sources are likely to contribute to the TE composition of

85   the bulk aerosol.

86   The objectives of this study were to (1) investigate aerosol sources of a suite of TEs of interest to

87   the GEOTRACES programme (www.geotraces.org); and (2) quantify the atmospheric deposition flux of

88   TEs to surface waters of the North Atlantic at latitudes greater than 40°N. In order to do this, TE fluxes

89   were calculated using, 1) the traditional approach of deriving fluxes from the summation of TE

3

90 concentration data from wet and dry deposition (e.g., Duce at al., 1991), and 2) a novel tracer approach

91 which uses the natural cosmogenic radionuclide Beryllium-7 (^{7}Be) as a tracer for atmospheric inputs

92 (Cámara-Mor et al., 2011; Kadko and Prospero, 2011; Kadko et al., 2015; 2016). The two approaches

93 resulted in flux estimates that were in excellent agreement for approximately half the TEs under

94 investigation, but performed less well for the remaining TEs, with differences of 2-40 times between

95 them. Therefore, potential sources of uncertainties are discussed.

96 **METHODS**

97   The *GEOVIDE* campaign (*GEOTRACES* cruise *GA01*; 15 May-30 June 2014), on board the *N/O*

98 *Pourquoi Pas?*, departed from Lisbon, Portugal, and sailed northwest following the *OVIDE* line

99 (http://wwz.ifremer.fr/lpo/La-recherche/Projets-en-cours/OVIDE) to the Greenland shelf, after which

100 the ship entered the Labrador Sea and sailed for the final port of St John's, Newfoundland, Canada (Fig.

101 1). In total, 18 aerosol samples and 10 precipitation samples were collected for the determination of a

102 suite of TEs. In addition, ^{7}Be was determined from 18 aerosol samples, 8 precipitation samples, and 9

103 relatively shallow water column profiles.
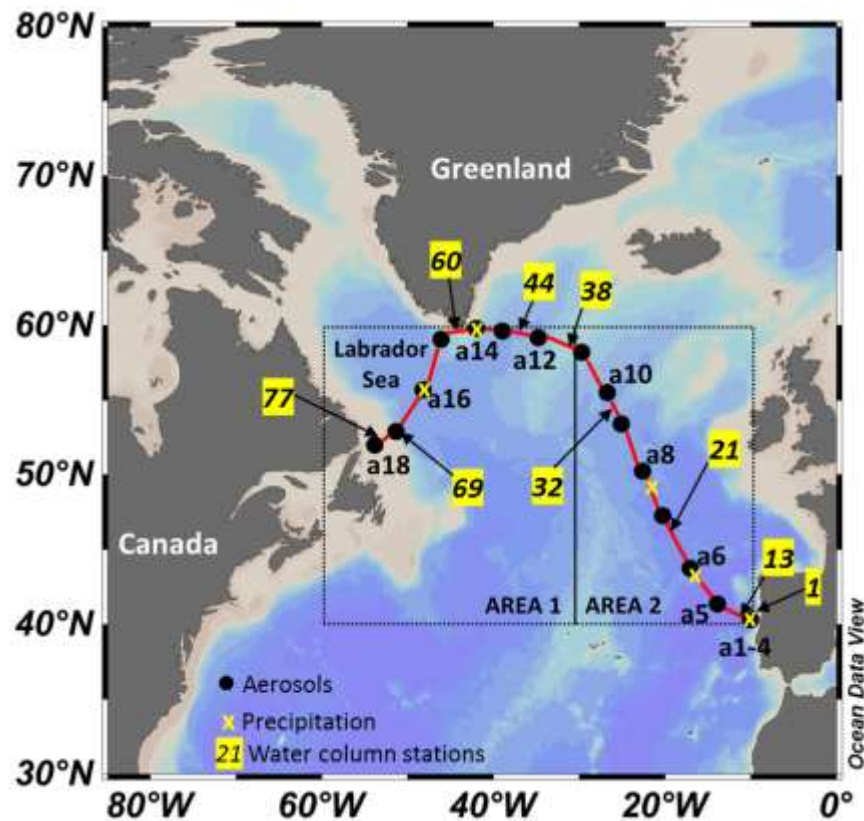
104

105   Figure 1. The *GEOVIDE* cruise track. Aerosol samples *geoa*1-4 (displayed as "a1-4") were collected in

106   close proximity, thus are only shown as one dot on the above map. There were ten precipitation events;

107   the first six occurred at the same location as aerosol samples *geoa*1-4. The dashed lines indicate the

108   boxes, Area 1 and Area 2; the dividing line is located at 30°W (further details can be found in the

109   Methods). Water column sampling stations are indicated by the arrows; the station numbers are

110   highlighted in yellow. Metadata for the aerosol,rain and water column sample locations can be found in

111   Tables S1, S2 and S3, respectively (Supplemental Material).

112

113   <u>Sample collection and analysis</u>

114   *Aerosol TEs*: Samples were collected using a mass flow-controlled, high volume aerosol sampler

115   ($\sim$1 m^{-3} min^{-1}; model TE 5171, Tisch Environmental). The aerosol sampler was sector ($\pm$ 60° from the

116   bow) and wind speed (<0.9 m s^{-1}) controlled, to minimise the risk of contamination from the ship's

117   exhaust stack, using an anemometer and vane attached to a 3 m pole mounted on the railings near the

118   aerosol sampler. The aerosol sampler was positioned on the forward railings (starboard side) on the

119   flight deck above the bridge ($\sim$15 m above sea level). Twelve replicate samples were collected on acid-

120   washed, 47 mm diameter Whatman 41 (W41) ashless filter discs (mixed cellulose esters; total exposed

121   area 149 cm^2), which were positioned on a 12-position PVC adapter plate (Shelley et al., 2015). The first

122   sample collected represented a 24 h deployment (sample time = 19.6 h), but after visual inspection of

123   the filters and of air mass back trajectory simulations (using the Hybrid Single Particle Lagrangian

124   Integrated Trajectory Model, HYSPLIT), it became apparent that this sampling duration would be

125   insufficient to collect enough material on the filters. Thus, the deployment time was increased to 48 h

126   (sample time = 17.4 – 47.6 h) for all subsequent samples. After recovery, filters were removed from the

127   filter holders inside a laminar flow bench, placed in individual petri-slides (Merck), double ziplock

128   bagged, and immediately frozen (-20 °C) for storage. Three of the twelve replicate samples were

129   reserved for determination of ^{7}Be.

130   On return to the home laboratory, the aerosol samples were digested to determine

131   concentrations of a suite of TEs by high resolution, magnetic sector field inductively coupled plasma

132   mass spectrometry (SF-ICP-MS; Element 2, Thermo-Fisher). The TEs determined were: Al, P, Ti, V, Cr,

133   Mn, Fe, Co, Ni, Cu, Zn, Sr, Y, Zr, Mo, Ag, Cd, Ba and Pb. This list includes lithogenic tracers (Al, Ti, Y, Zr), a

134   suite of bioactive elements (P, V, Cr, Mn, Fe, Co, Ni, Cu, Zn, Mo, Cd), and pollution-derived TEs with no

135   known biological role (Ag and Pb). All filter digestions were performed under Class-100 laminar flow

136   conditions following the protocol of Morton et al. (2013). Briefly, the W41 filter discs were digested in

137   tightly-capped 15 mL Teflon-PFA vials (Savillex) using sequential additions of (1) 500 µL of nitric acid

138   (HNO_3; 15.8 M, Ultrapur, Merck); and (2) 1 mL of HNO_3 (15.8 M, Ultrapur, Merck) plus 200 µL of

139   hydrofluoric acid (HF; 32 M, Ultrapur, Merck). During both steps the solutions were heated to 150 °C,

140   and were taken to near-dryness after each step. After the final digestion and evaporation, the samples

141   were re-dissolved in 15 mL of 0.4 M HNO_3 (Ultrapur, Merck) containing 1 ppb indium (In) as an internal

142   standard for drift correction. For analysis by SF-ICP-MS, 2 mL of this solution was further diluted in acid-

143   washed, rounded bottom, polypropylene centrifuge tubes (VWR) by addition of 2 mL of the same batch

144   of 0.4 M HNO_3 containing 1 ppb In. Samples were introduced to a PFA-ST nebulizer (Elemental Scientific

145   Incorporated) via a modified SC-Fast introduction system consisting of an SC-2 autosampler, a six-port

146   valve and a vacuum rinsing pump. Blank solutions for the acid digestions were prepared by digesting

147   W41 discs that had been deployed in the aerosol sampler for 1 h while the pumps were not in

148   operation, and the resulting concentrations were subtracted from all acid-digested filter samples. Blank

149   values can be found in Table S1 (Supplemental Material).

150   In order to assess the homogeneity of the twelve replicate sample filters every fourth sample

151   was analysed in triplicate. For Fe, for example, this resulted in precision (relative standard deviation

152   between replicate samples) that was less than 10% for all but the lightest-loaded sample (0.68 ± 0.19 ng

153   m^{-3}), which was close to the detection limit. In order to investigate digestion efficiency and recovery,

154   two separate reference materials were digested. The reference materials digested were: National

155   Research Council of Canada lake sediment (LKSD-1; composition data compiled in the GeoReM

156   database; http://georem.mpch-mainz.gwdg.de/); and Arizona Test Dust (ATD; nominal 0-3 µm, Powder

157   Technology Inc.). The Landing Laboratory at Florida State University is currently investigating the use of

158   ATD as a dust reference material, and is compiling a database of elemental abundances. The ATD will

159   become more suitable for distribution as a dust reference material as other laboratories contribute

160   concentrations to the consensus reference material effort (sub-samples are available on request from:

161   wlanding@fsu.edu). Further discussion of the use of ATD as a reference material, and elemental

162   abundance data is presented in Table 1 of Shelley et al. (2015). Values for LKSD-1 and ATD from this

163   study are presented in Table S1.

164   *Precipitation TEs*: Rain samples were collected on an event basis using a Teflon precipitation

165   sampler that was fabricated in-house at the Laboratoire des sciences de l'Environnement MARin

166   (LEMAR; Cheize et al., 2012). An acid-cleaned 1 L HDPE bottle was attached to the sampler by means of

167   a Teflon screw fitting. The cover of the rain sampler was removed manually on commencement of a rain

168   event, and replaced after the rain had stopped. The sample was immediately removed from the sampler

169   and the sample bottle replaced with a new, clean 1 L bottle. Samples were acidified to 0.024 M HCl

170   (Ultrapur, Merck) inside a laminar flow bench at sea, and double bagged for storage. On return to the

171   home laboratory, the samples were shaken vigorously, and ~2 mL of sample was pipetted in to Teflon

172   beakers. The aliquot was evaporated on a hotplate positioned inside a laminar flow bench. The resulting

173   residue was re-dissolved in 4 mL 0.4 M HNO_3 (Ultrapur, Merck) prior to determination by SF-ICP-MS of

174   the same suite of TEs as the aerosol samples (except strontium (Sr) and silver (Ag) which were not

175   determined in the precipitation samples). Precipitation sample volumes ranged from 13-1120 mL. The

176   TE concentration data and metadata for the precipitation samples can be found in Table S2

177   (Supplemental Material).

178   *Determination of ^{7}Be in seawater, bulk deposition (precipitation) and aerosol samples:* Seawater

179   samples (n=28, 50-100 L each) were collected from three to four depths spanning from the surface (5 m)

180   to about 100 m below the mixed layer (Fig. S2, Supplemental Material), using a stainless steel CTD

181   rosette and standard Niskin bottles equipped with rubber feathers instead of steel springs. Bulk

182   deposition samples (n=8, 0.16-2.6 L each) were collected over one to eight day intervals, depending on

183   the sample volume and the proximity to water column stations, using a homemade bulk deposition

184   sampler (1.5 m high, 25 cm diameter) similar to the one used for TE precipitation collection. The ^{7}Be

185   bulk deposition sampler was positioned close to the TE precipitation sampler to ensure similar sampling

186   conditions. However, in contrast to the TE precipitation collections, which were on an event basis to

187   minimise the risk of contamination, the ^{7}Be bulk deposition samplers remained open and uncovered at

188   all times. Seawater and precipitation samples were treated following the protocols of Cámara-Mor et al.

189   (2011). Briefly, samples were acidified with 37% HCl (Panreac/QP) to pH ~1 and spiked with 5 mg of

190   stable Be as a yield tracer. After addition of Fe^{3+} as a carrier and vigorous stirring, samples were allowed

191   to equilibrate for 12 h. Beryllium was then co-precipitated with iron hydroxides by adjusting the pH to

192   ~8.5 using 30% NH_3 (Panreac/QP). The supernatant was carefully removed via siphoning and the

193   precipitate was transferred to 250 mL plastic bottles and stored until further analysis at the Universitat

194   Autònoma de Barcelona (UAB). Aerosol samples (n=18) were collected as described above for TEs and

195   stored frozen until determination of ^{7}Be. At the UAB, Fe precipitates from seawater and precipitation

196   samples were dissolved in 2 M HCl (Panreac/QP) and transferred to hermetically sealed PE vials for

7

197   gamma counting. ^{7}Be gamma emissions (478 keV) were measured using well-type, high-purity Ge

198   detectors within three months of collection. Detectors were calibrated for the correct vial geometry by

199   measuring a commercial standard solution (MCR-2009-018) of known gamma activities (60 – 1836 keV).

200   For aerosol samples, the three filters were processed together. Each set of three filters was spiked with

201   2 mg of stable Be as a yield tracer, digested using a mixture of concentrated HNO_3, HCl and HF at a ratio

202   of 10:4:6 (Panreac/technical and analytical grade), re-dissolved with 2 M HCl, placed in vials and

203   measured by gamma spectrometry as described for the seawater and precipitation samples. After

204   counting, one aliquot from each sample was taken to determine the chemical recovery of stable Be by

205   inductively coupled plasma optical emission spectrometry (ICP-OES), which averaged 88%. ^{7}Be activities

206   were corrected for decay to collection date. The ^{7}Be data and metadata for aerosol, precipitation and

207   seawater samples can be found in Table S3 (Supplemental Material).

208   Air mass back trajectories

209   Five-day (120 h) air mass back trajectories were simulated for each aerosol sampling interval

210   (Fig. S1, Supplemental Material) using the GDAS meteorology in the publicly available NOAA Air

211   Resources Laboratory Hybrid Single-Particle Lagrangian Integrated Trajectory (HYSPLIT) model (Stein et

212   al., 2015; Rolph, 2016). The normal form of the model was used, with arrival heights of 50, 500 and 1500

213   m, in order to investigate the behaviour and fate of aerosols in and above the MBL, typically 400–1200

214   m thick). With the exception of samples *geoa*9, *geoa*16-18 (European and Canadian origins,

215   respectively), all air mass back trajectories during this study were defined as Remote Marine, meaning

216   that the air masses had had little to no interaction with major continental land masses within the

217   simulation period.

218

219   Positive matrix factorisation (PMF)

220   Multivariate statistical analysis methods provide a powerful tool for looking at patterns in large

221   data sets and/or datasets that include many parameters. Receptor models use multivariate statistical

222   techniques that can be used to identify and quantitatively apportion pollutants to their sources by

223   looking for trends, and identifying potential markers for the sources (Comero et al., 2009). The United

224   States Environmental Protection Agency (EPA) has developed a receptor model for analysis of

225   environmental quality data that is freely available online (available at: http://www.epa.gov/air-

226   research/positive-matrix-factorization-model-environmental-data-analyses). Positive Matrix

227 Factorisation (PMF) reduces the dimensions of complex data sets to a smaller number of factors, which

228 are used to identify potential sources.

229 Although the US EPA environmental quality monitoring sites are at fixed locations (as opposed

230 to multiple sites along an oceanographic transect), PMF may still be able to provide insights into

231 potential aerosol sources, especially when used in conjunction with air mass back trajectory simulations

232 and enrichment factors. The EPA PMF model (v. 5.0) was used in this study to look for trends in the

233 *GEOVIDE* aerosol TE data set. A detailed description of how to interpret the model outputs and error

234 estimation results can be found in the EPA PMF user guide (http://www2.epa.gov/sites/production/files

235 /2015-02/documents/pmf_5.0_user_guide.pdf). Briefly, "Base Model Runs" produce the primary output

236 of profiles and factor contributions. The base model run uses a random seed (starting point) for

237 iterations, and generates a value for goodness of fit; the Q-value. The iteration with the lowest Q-

238 (robust) value is highlighted in the output, and the analysis based on this iteration should be used to

239 interpret the model output.

240 Although the EPA-PMF model cannot conclusively define the sources represented by the factors,

241 it does allow the user to identify markers for the sources based on *a priori* knowledge of potential

242 aerosol sources (e.g., lithogenic TEs such as Al and Ti for mineral dust, or V and Ni for shipping

243 emissions). The application of the EPA-PMF model in this study was exploratory, in the sense that all

244 data was included without any attempt to weight individual data points identified as outliers. However,

245 sample *geoa*16 and 18 were excluded from the PMF analysis, due to concentrations below the detection

246 limit for Cr, Y and Zr (*geoa*16), and Ni and Zn (*geoa*18), as the model is unable to process blank cells, and

247 it is inappropriate to interpolate aerosol TE data. Samples were removed rather than TEs to maximise

248 the number of TEs that could serve as markers for source apportionment. A two, three and four factor

249 model was fitted to the aerosol TE data. However, due to the small number of samples only the two

250 factor model was well-constrained in terms of error estimation. The two factors were identified as: (1)

251 mineral dust (highest contributions from Zr and Y), and (2) a factor that was dominated by Sr, but also

252 had high contributions from Cu, V and Ni.

253

254 Atmospheric deposition flux estimations

255 The atmospheric deposition of trace elements to the ocean is a key parameter in

256 biogeochemical models, yet it remains poorly constrained, largely as a result of the difficulty in

257   collecting representative samples from remote oceanographic settings, and the challenge of converting

258   aerosol chemical concentration data into realistic flux estimates. In the Atlantic Ocean, chemical

259   composition data has been collected from both island-based sites, e.g., from long-term atmospheric

260   observatories, such as the AEROCE sites in the North Atlantic Ocean (Bermuda, Barbados, Mace Head,

261   Izaña; e.g. Prospero et al., 2014; Sholkovitz et al., 2009), and from large-scale oceanographic campaigns,

262   such as the Atlantic Meridional Transect (Baker et al. 2006; 2013), *CLIVAR* Repeat Hydrography cruises

263   (Buck et al., 2010) and *GEOTRACES* cruises (Shelley et al., 2015), as well as from numerous regional-scale

264   oceanographic campaigns (e.g. Stuut et al., 2005).

265   As atmospheric deposition is both spatially and temporally variable, in order to minimise the

266   effect of outliers in the aerosol chemical concentration data we have chosen to take a box approach to

267   estimate atmospheric deposition fluxes over our study area in late spring/early summer 2014. We base

268   our atmospheric deposition boxes on the areas defined in Baker et al. (2010), which they based on the

269   distribution of rainfall over the Atlantic Ocean (Xie and Arkin, 1997). However, as this study occupied

270   stations further north than Baker et al. (2010), we have extended the boxed regions by approximately

271   10° in a northerly direction to include the most northerly section of our study area. Therefore, the

272   regions we define are Area 1 (western section of transect, >30°W) and Area 2 (eastern section of

273   transect, <30°W) (Fig. 1).

274

275   <u>Dry deposition flux estimation</u>

276   Dry deposition fluxes of TEs, F_{dry}, were calculated using the following equation:

$$F_{dry} = C_{atmos} \times V_d$$

277   [1]

278   Where C_{atmos} is the concentration of the species of interest in the aerosol, and V_d is the dry

279   deposition velocity. The largest source of error (up to a factor of 3) in this calculation is associated with

280   the choice of V_d (Duce et al., 1991). Deposition velocity is sensitive to fluctuations in wind speed, relative

281   humidity and particle size (Slinn and Slinn, 1981), and while wind speed and particle size dependent

282   parameterisations are available (e.g. Ganzeveld et al., 1998), these, too, are subject to uncertainties. As

283   a result, fixed V_d values are still commonly used.

284

285   <u>Wet deposition flux estimation</u>

286   Wet deposition TE fluxes, F_{wet}, were calculated using the following equation:

$$F_{wet} = C_{rain} \times P_R$$

287   [2]

288   Where C_{rain} is the concentration of the element of interest in rain water and P_R is the

289   precipitation rate. However, accurate representation of precipitation rates can be problematic in remote

290   ocean regions. Rain collector efficiency is very sensitive to wind speed, thus, in order to obtain accurate

291   rainfall rates wind screens are required (Sieck et al., 2007). This presents a significant obstacle to

292   determining accurate precipitation rates from samples collected at sea, where samplers are located on

293   exposed platforms high on the ship, and sampling occurs while the ship is facing into the oncoming wind

294   and/or while underway, as wind screens are not routinely deployed on rain samplers at sea.

295   Furthermore, rain samples are usually only collected from events that occur along the planned cruise

296   track, consequently nearby events are missed, as are ones that occurred prior to station occupation.

297   Other sources of wet deposition, such as fog and snow can be difficult to collect, and their deposition

298   rates may be even more difficult to quantify than rain rates. Thus, researchers may rely on climatologies

299   from satellite products, which, themselves, may be subject to large uncertainties. With this in mind, the

300   precipitation data used in this study was obtained from the NASA Giovanni satellite data product

301   (http://giovanni.sci.gsfc.nasa.gov/giovanni/) using TRMM and GPM sources. A time-averaged (May-June

302   2014) map of multi-satellite precipitation estimates, with 0.1° resolution was used in combination with a

303   plot of area-averaged precipitation rate estimates for the eastern section of the study area (Figs. S2a

304   and S2b, Supplemental Material), resulting in precipitation rate estimates from 0-3.6 mm d^{-1} along the

305   cruise track (Fig. S3a). For the wet deposition flux estimates we chose a value close to the mid-point of

306   this range, 2.0 mm d^{-1}. This value was also chosen as it reflects the low end of the range of precipitation

307   rates determined from the ^{7}Be precipitation collections (2.2-6.7 mm d^{-1}). This value corresponds to the

308   low end of the range of precipitation rates determined from the ^{7}Be precipitation collections.

309   An additional source of error in wet deposition flux estimations may result from the sensitivity

310   of species concentration on sample volume, due to a dilution effect (Jaffrezo et al., 1990). Therefore, to

311   mitigate any volume effects, we calculated a volume weighted mean (VWM) rain concentration (C_{rain}) for

312   each of the two boxed areas used in this study, from the product of the rainfall concentrations (C_i) and
313   volumes (V_i) (Eq. 3).

$$C_{rain} = \sum C_i V_i \ / \ \sum V_i$$

314

315   [3]

316   <u>Total deposition flux estimation (^{7}Be approach)</u>

317   An alternative to the traditional approach for the estimation of the total deposition fluxes of TEs
318   (summed wet and dry deposition fluxes) described above is the use of ^{7}Be as a proxy for atmospheric
319   deposition as described by Kadko et al. (2015; 2016). This cosmogenically-formed radioisotope ($T_{1/2}$ of
320   53.3 days) is deposited to the ocean predominantly via precipitation, and is subsequently homogenised
321   in the mixed layer (Silker, 1972; Kadko and Olson, 1996). As the water column inventory represents an
322   integration of the input over approximately the previous 2.5 months (the mean life-time of ^{7}Be is 77
323   days), ^{7}Be can be used as a tracer of atmospheric deposition on seasonal timescales. This approach
324   assumes that the only loss term for ^{7}Be from the water column is radioactive decay.

325   The total deposition fluxes of the species of interest are derived from the following equation,
326   using ^{7}Be as an example:

$$F_{total, \ Be7} = \ C_{Be7} \times (P_R \times S_R \times \rho + V_d)$$

327   [4]

328   Where the total deposition flux of ^{7}Be (dpm m^{-2} d^{-1}), $F_{total, \ Be7}$, is derived from the ^{7}Be inventory in
329   the upper water column (dpm m^{-2}, ocean ΣBe7) multiplied by the ^{7}Be radioactive decay constant (λ =
330   0.013 d^{-1}), and C_{Be7} is the concentration of ^{7}Be in the bulk aerosol (dpm m^{-3}). The inventory of ^{7}Be in the
331   mixed layer was calculated considering a homogeneous concentration of ^{7}Be and a mixed layer depth
332   set by the threshold method (taking a threshold value difference of 0.05 kg m^{-3} for the potential density
333   anomaly referenced to the sea surface, Monterey and Levitus, 1997; Thomson and Fine, 2003). Below
334   the mixed layer, the inventory of ^{7}Be was calculated assuming an exponential decrease from the base of
335   the mixed layer to the depth where the ^{7}Be concentration was 1% of that in the mixed layer. P_R is the
336   precipitation rate (m d^{-1}), S_R is the scavenging ratio, and ρ is the density of liquid water divided by the

337   density of air (~1000 kg m^{-3}/1.2 kg m^{-3} = ~833). The first three terms in the brackets of Equation 4, P_R, S_R

338   and ρ, describe the wet deposition velocity, whereas V_d is the dry deposition velocity (m d^{-1}); when

339   summed these terms describe the bulk deposition velocity. As the open ocean is generally a low particle

340   regime, $T_{1/2}$ of ^{7}Be is short and atmospheric inputs are relatively large, losses via particle scavenging in

341   the water column are assumed to be negligible. Thus, Equation 5 is an alternative way of writing

342   Equation 4.

$$F_{total,\ Be7} = ([Ocean\ \Sigma Be7]\lambda) = C_{Be7} \times Bulk\ V_d$$

343

344   [5]

345   Similarly, we can calculate the flux of atmospheric TEs ($F_{total,\ TE}$) from the bulk V_d (P_R x S_R x ρ + V_d)

346   and the concentration of TE (C_{TE}) in aerosol (Eq. 6).

$$F_{total,\ TE} = C_{TE} \times Bulk\ V_d$$

347   [6]

348   Assuming that the bulk V_d is the same for both TEs and ^{7}Be, we can then estimate the flux of any

349   aerosol TE from the ocean inventory of ^{7}Be and the TE/^{7}Be ratio in aerosols (Eq. 7).

$$F_{total,TE} = ([Ocean\ \Sigma Be7]\lambda) \times \frac{C_{TE}}{C_{Be7}}$$

350   [7]

351   Is it reasonable to assume the bulk V_d is the same for TEs and ^{7}Be? Table 1 shows that while the

352   S_R for mineral dust (represented by Al in Table 1) is relatively small, V_d is relatively large, whereas for

353   ^{7}Be, the opposite is true, thus differences tend to cancel. Jickells and Spokes (2001) estimated a mean S_R

354   for Fe of 200, and Duce et al. (1991) found that the global mean for both Al (lithogenic) and Pb

355   (pollution-derived) was also 200, and, thus, assumed that this value would hold for other TEs in the

356   Atlantic. In contrast, Akata et al. (2008) found that the mean S_R for ^{7}Be was 640, and the V_d ranged from

357   147-10368 m d^{-1} (0.17-12 cm s^{-1}). In Table 1, we have used a V_d of 294 m d^{-1} (0.34 cm s^{-1}) as ^{7}Be is

358   primarily associated with fine mode particles, with a mean size range of 0.5-0.6 µm (Winkler et al.,

359   1998). Thus, Equation 4 allows us to estimate the differences in the bulk V_d term between coarse and

360 fine mode aerosols (Table 1). The bulk V_d for Al was roughly equal to that of [7]Be for precipitation rates of

361 ~1-3 mm d^{-1}, which cover the range of precipitation rates estimated for the study area in May/June 2014

362 from the Giovanni satellite products (Fig. S2, Supplemental Material), but is less than that of [7]Be for the

363 precipitation rates estimated from the [7]Be precipitation collections (2.2-6.7 mm d^{-1}). This reflects the

364 higher scavenging ratio of [7]Be relative to that of Al.

365 Table 1. Bulk deposition velocities (P_R x S_R x ρ + V_d) for mineral dust (e.g. Al) and [7]Be over the
366 precipitation rate range 0.5-7 mm d^{-1}.

	Al	[7]Be	
S_R	200[a, b]	640[c]	
V_d (m d^{-1})	1000[a]	294[c]	
P_R	Bulk V_d	Bulk V_d	Al/[7]Be bulk V_d
mm d^{-1}	m d^{-1}	m d^{-1}	ratio
0.5	1083	560	1.9
1	1167	827	1.4
2	1333	1360	1.0
3	1500	1893	0.8
4	1667	2427	0.7
5	1833	2961	0.6
6	2000	3494	0.6
7	2167	4027	0.5

[a]Duce et al. (1991)
[b]Jickells and Spokes (2001)
[c]Akata et al. (2008)

367

368 The total deposition flux of [7]Be was also estimated from precipitation samples (Table 2c), F_{total}

369 $_{(precipitation), Be7}$, by using the [7]Be activity decay-corrected to mid sampling (A_{Be7}), the time period of

370 collection (t) and the collector surface (S) as shown in Equation 8. The precipitation samples are

371 representative of short periods of time (from 1 to 8 days), while the inventories measured in the water

372 column integrate over the mean life-time of [7]Be.

$$F_{total\ (precipitation),\ Be7} = \frac{A_{Be7} \times \lambda}{(1 - e^{-\lambda t}) \times S}$$

373 [8]

374 **RESULTS AND DISCUSSION**

375 Aerosol TE distributions

376   The lithogenic TEs, Al, Mn, Fe, Ti, Y and Zr, all had similar spatial distributions (Fig. 2; Table S1,

377   Supplemental Material), suggesting common source(s) and atmospheric processing during transport.

378   Both Al and Ti can be used as proxies for mineral dust inputs as it is assumed that they are mostly

379   associated with mineral phases. Given that the abundance of Al and Ti in mean upper crustal (UC)

380   material (a proxy for a mineral dust end member) is known, 8.2±3% and 0.38±0.05%, respectively

381   (Rudnick and Gao, 2003), the abundance of either Al or Ti can be used to estimate total dust

382   concentrations. Throughout the *GEOVIDE* campaign aerosol Ti loading was low (0.0084–1.9 ng Ti m^{-3} air

383   filtered; Fig. 2), and, thus by implication, so too was dust loading. Using the Ti data, this results in

384   estimates of ~2-500 ng of material per m^{-3} air filtered. The region of lowest aerosol Ti and dust loading

385   was in the Southwest Irminger Sea and the Labrador Sea (*geoa*12-16, Ti = 0.0084-0.14 ng m^{-3}). As the

386   ship passed on to the Newfoundland shelf aerosol Ti loading, and therefore, atmospheric dust loading

387   increased.

388
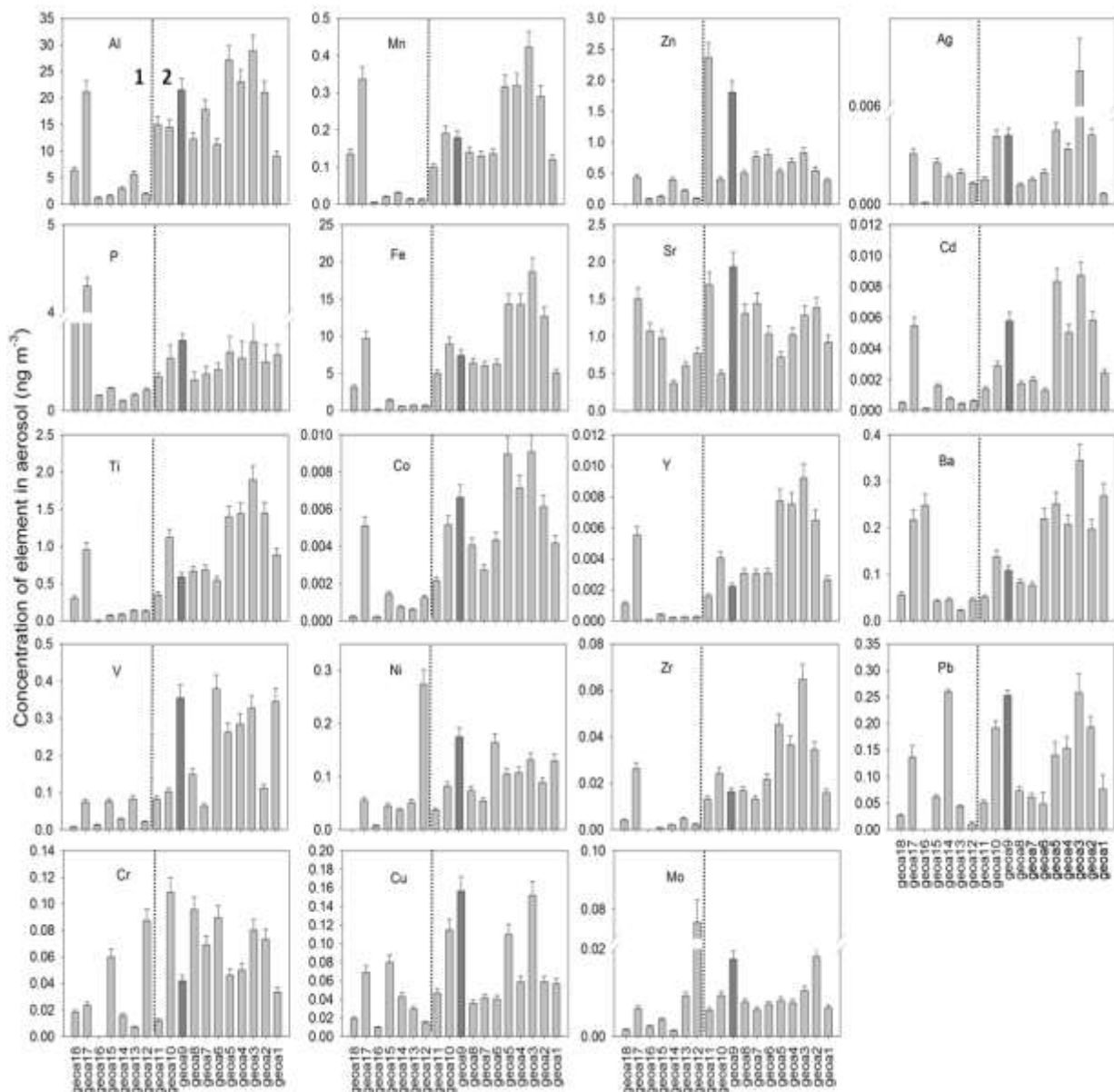
Figure 2. Aerosol TE concentrations (ng m^{-3}) ± 1 SD. The x-axis is reversed to reflect the longitude of the

sample locations, i.e. west-east. Sample *geoa*9 is patterned to facilitate identification in these plots, and

the boundary between Areas 1 and 2 is marked by a dashed vertical line. The data is displayed in Table

S1 (Supplemental Material) and is available on request from the corresponding author or the LEFE-

CYBER database (http://www.obsvlfr.fr/proof/php/*GEOVIDE*/*GEOVIDE*.php).

Nickel, Cu, Sr, Mo, Ag and Pb had no clear spatial patterns, suggestive of either one discrete

source with variable inputs (e.g., sea salt), or multiple sources (e.g., different industrial sources) along

the transect and, with the exception of Sr, likely of primarily anthropogenic origin. The lack of a spatial

16

397   pattern for Sr deposition could point to a marine source of Sr (Vitousek et al., 1999). However, there was

398   no relationship between the average wind speed and aerosol Sr (r^2 = 0.20, p = 0.074; Fig. S4,

399   Supplemental Material), suggesting that the Sr during GEOVIDE was not predominantly a cyclic salt (Nair

400   et al., 2005).

401   　　　The influence of different source regions on aerosol TE composition can result in large

402   differences in TE concentrations in aerosol samples collected in similar areas. For example, the aerosol

403   Al and Fe concentrations in samples collected at 40.3°N, 10.0°W (*geoa*1) and 40.3°N, 12.2°W (*geoa*2)

404   during this study were 9.0 and 21 ng m^{-3} (Al), and 5.1 and 13 ng m^{-3} (Fe), respectively, and five days prior

405   to sampling the air mass had originated over southern Greenland. In contrast, during the *GEOTRACES*

406   *GA*03 campaign (leg 1, Oct-Nov 2010, Lisbon, Portugal to Mindelo, Cape Verde Islands) an aerosol

407   sample was collected from a nearby location (38.3°N, 9.7°W), which had 1-2 orders of magnitude higher

408   Al and Fe (155 and 147 ng m^{-3}, respectively). An air mass back trajectory simulation of that sample

409   indicated that the sampled aerosol had been transported in an air mass that had previously traversed

410   much of northern and western Europe (Shelley et al., 2015).

411   　　　As atmospheric aerosol loading was low, compared to regions to the south of our study area

412   (i.e., under the influence of the Saharan dust plume, e.g., Shelley et al., 2015), all but one of the samples

413   (*geoa*9) had no visible material on the filters. Grey material was observed on the filters of sample *geoa*9,

414   which had a western European origin within five days of sample collection (Fig. S1, Supplemental

415   Material). This sample had higher concentrations (i.e., >1 SD higher) for about half of the TEs (Al, V, Co,

416   Ni, Cu, Zn, Sr, Mo, Cd, Pb), with respect to the previous and following samples (Fig. 2). Most of these TEs

417   (V, Ni, Cu, Zn, Mo, Cd, Pb) are linked with anthropogenic sources, which suggests that aerosol Al, Co and

418   Sr could also have had an anthropogenic component in this sample.

419   Aerosol elemental ratios and enrichment factors

420   　　　Although Al and Ti are equally suited as tracers of mineral dust inputs, it was decided to use Ti in

421   this study, as Ti is less prone to contamination from metal components on the ship. The very low Ti

422   loading (0.0084 ng m^{-3}) of sample *geoa*16 (close to the detection limit) could explain the anomalously

423   high TE/Ti ratios for some elements (Al, P, Zn, Sr, Ba, Pb). For example, the EF of Sr was 127 compared to

424   an average of 3.0±3.3 for the remaining samples (Table S4). This was less of a problem for the data

425   normalised to Al, but it should be noted that for Sr, Ba and Pb the elemental ratios were still

426   anomalously high for *geoa*16 whether the data was normalised to Al or Ti. Alternatively, sample *geoa*16

427   may have been contaminated for the TEs with anomalously high elemental ratios. Whatever the reason,

428   these anomalously high elemental ratios resulted in the decision to exclude this sample from the

429   following discussion.

430   In addition to similar spatial distributions, an Fe/Ti elemental mass ratio close to mean UC (10.2

431   ± 1.1; Rudnick and Gao, 2003) also suggests a common crustal source for these two elements. Indeed, a

432   strong correlation is often observed between Fe and other lithogenic TEs such as Ti in aerosol

433   concentration data (this study, r^2 = 0.95, P < 0.001) (Fig. 3A). However, as there is some degree of

434   variability in elemental abundances in crustal material (e.g., 13 and 11% variability for Ti and Fe,

435   respectively; Rudnick and Gao, 2003), mineral dust source materials can have elemental ratios that

436   significantly differ from the UC mean. In this study, the average (± 1 SD) Fe/Ti mass ratio was 10.5 ± 4.5

437   (Table S4, Supplemental Material), which does not vary significantly from the mean UC ratio, although

438   the range was large (5.0-22.0; Fig. 3B, Table S4). This situation could be due to non-lithogenic inputs of

439   Ti where the ratio was low, and non-lithogenic inputs of Fe where the ratio was high (i.e. variations in

440   the Fe/Ti ratios in the source material). It is less likely to be due to depletion of one metal with respect

441   to the other during atmospheric transport and deposition.

442   Given the distance covered, from Portugal to Greenland to Newfoundland (approximately 6000

443   km), it is not hard to imagine that different mineral phases would comprise the bulk aerosol in different

444   parts of the North Atlantic basin, and that these would be reflected by differences in the elemental

445   ratios. Indeed, the Fe/Ti ratios fall into four loose groups: (1) Newfoundland shelf = 10.3 ± 0.2 (*geoa*17-

446   18, longitudes >48°W); (2) Labrador Sea = 20.7 ± 1.8 (*geoa*15-16); (3) SW Irminger Sea = 5.7 ± 1.1

447   (*geoa*12-14); and (4) Area 2 = 9.9 ± 2.3 (*geoa*1-11). There is more variability (RSD ~20%) in the third and

448   fourth groups than the other two groups, but none of the ratios were identified as outliers by a Grubb's

449   test at the 95% confidence level. However, samples *geoa*9 and 11 had relatively high Fe/Ti ratios (13 and

450   14 respectively), and air mass back trajectories over the UK (Fig. S1, Supplemental Material), which

451   suggests that industrial emission aerosols produced in the UK/western Europe could have become

452   entrained with mineral dust, thus driving the Fe/Ti ratio up.

453

454
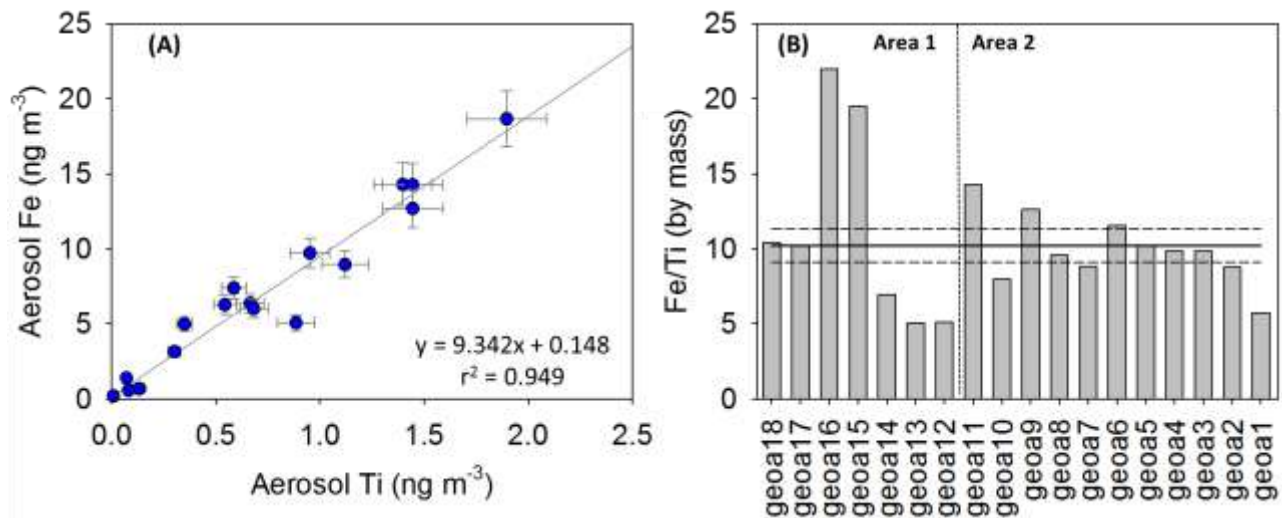
455

456 Figure 3. The linear relationship between aerosol Fe and Ti (A), the mass ratio of Fe/Ti (B), the solid

457 horizontal line represents the mean mass ratio in UC of 10.2 ± 1.1 (± 1 SD is indicated by the horizontal

458 dashed lines; Rudnick and Gao, 2003)

459   TEs are frequently enriched in industrial emission aerosols compared with natural crustal

460 abundances (e.g. Gelado-Caballero et al., 2012). Enrichment factors (EFs) are calculated by dividing the

461 ratio of a TE to a lithogenic tracer (e.g. TE/Ti) in the sample by the same ratio in a reference crustal

462 material (e.g. upper crust, Rudnick and Gao, 2003). In this way, EFs may be used to suggest whether

463 aerosol TEs are sourced from mineral dust or from anthropogenic activities, such as metal smelting or

464 fossil fuel combustion. Due to the natural variability of TE abundance in crustal material we only

465 consider EFs >10 as significantly enriched. As expected, the primarily lithogenic TEs, Al, Mn, Fe, Co, Y, Zr

466 and Ba, had EFs <10 for all samples. Mixed-sourced TEs (those having mineral dust, and anthropogenic

467 sources) had median EFs <10 (3.4, 8.2, and 2.4 for P, V and Cr, respectively), plus 2-5 samples with EFs

468 >10. Ni and Cu also had median values close to 10 (8.8 and 11, respectively), so can also be described as

469 mixed-source here. The remaining TEs, Zn, Sr, Mo, Ag, Cd and Pb, all had median values >10, and with

470 the exception of Sr and Ag, no samples with EFs <10 (Fig. 4). With the exception of Sr, this group of

471 elements are likely to be primarily derived from pollution sources. Vitousek et al (1999) argue that most

472 aerosol Sr over the open ocean is sourced by sea salt. However, Sr in seawater is 10^6 more abundant

473 than Ti (i.e. μmol kg^{-1}, compared to pmol kg^{-1}) (de Villiers, 1999; Dammshäuser et al., 2013), which

474 results in an elemental mass ratio seven orders of magnitude higher than the crustal ratio. Given that

475 the range of Sr/Ti EFs in this study was 5.3-164, the EFs suggest that the dominant source of Sr was

476 terrestrial, with sea salt likely contributing in the case of significant enrichment. This is consistent with

477   the observation that the Sr/Ti ratios were generally lower (with the exception of *geoa*10) closer to

478   continental landmasses (Table S4, Supplemental Material).

479
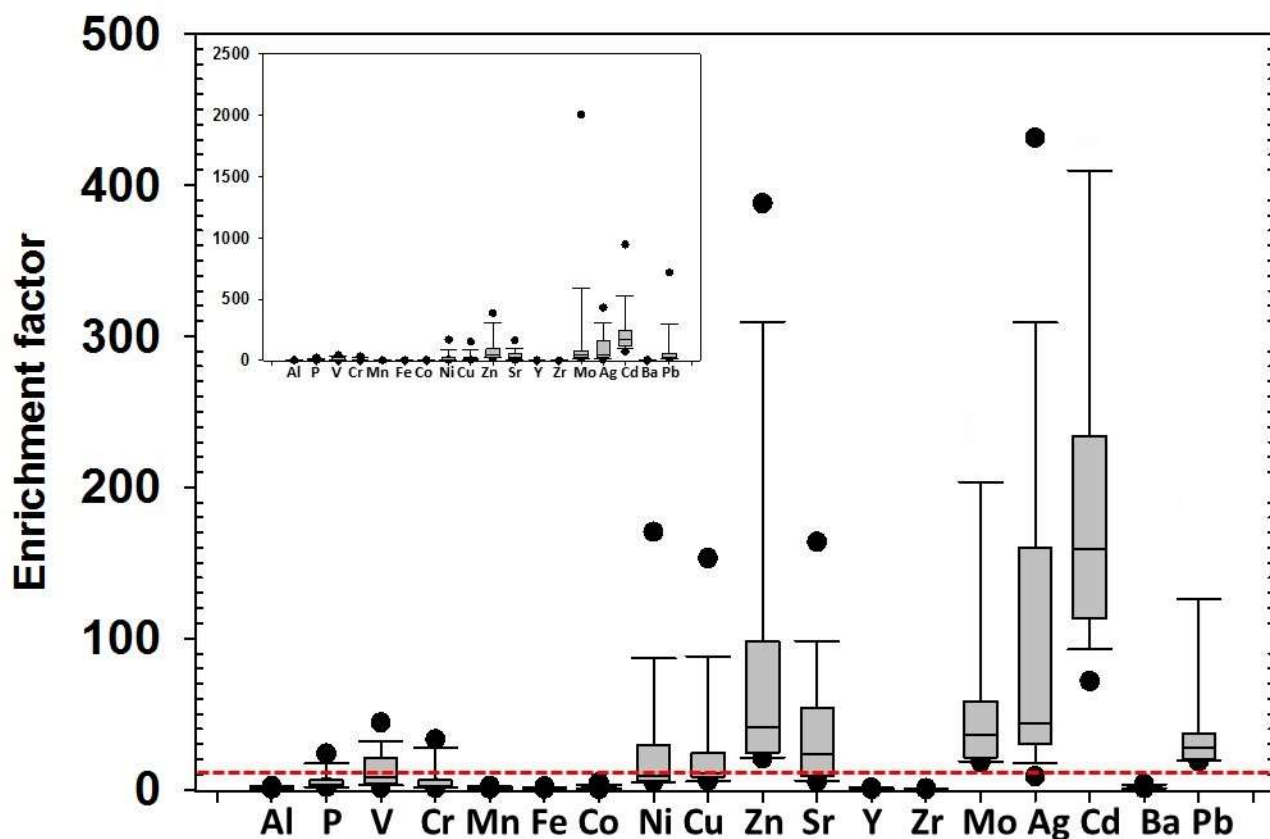
480

481   Figure 4. Box and whisker plots of enrichment factors (EFs; normalised to Ti). Outliers are marked with

482   black dots, and the line in the box is the median value. The inset plot includes all data, except sample

483   *geao*16. The main plot excludes the three EFs> 500 (Mo, Cd and Pb). The red dashed line indicates an EF

484   of 10; data above this line are considered significantly enriched.

485

486   Positive matrix factorisation (PMF)

487   The use of PMF was explored as an alternative to enrichment factors for categorising aerosol

488   source apportionment. The EPA-PMF output suggests that the GEOVIDE aerosol TE data can be

489   described by just two factors (Fig. 5). Factor 1 is dominated by Zr (100% of the variability in the aerosol

490   Zr data is explained by this factor). In addition, > 90% of Ti, Mn, Fe, Ag, and Y, and 88.5% of Al is

491   described by Factor 1. This combination of primarily lithogenic TEs (exception Ag) suggests that Factor 1

492   represents a mineral dust source. This factor is relatively more dominant early in the cruise close to the

493   Iberian Peninsula (samples *geoa*2-5), and on the Newfoundland shelf (*geoa*17). Factor 2 is dominated by

494   Sr (99.7% of the variability in aerosol Sr is explained by Factor 2), which is also primarily lithogenic,

495   based on the calculated EFs. However, Factor 2 also had high contributions from V, Ni and Cu (72.8%,

496   76.7% and 73.7%, respectively, and was most important from ~53.4-55.5°N (*geoa*9), so may also have an

497   anthropogenic component given that these four elements all show some degree of enrichment (25, 24,

498   37 and 40 for V, Ni, Cu and Sr, respectively) at this location. For example, V and Ni are particularly

499   enriched in exhaust emissions from marine engines using heavy fuel oils, and to a lesser extent so are Zn

500   (50% in Factor 2) and Cu (Celo et al., 2015; Streibel et al, 2016). The non-ferrous metal production

501   industry is also an important source of Cu (Pacyna and Pacyna, 2001). In addition, these TEs are also

502   present in mineral dust (e.g. Shelley et al., 2015). Thus, it seems likely that this factor represents a mixed

503   dust source, comprised of a combination of minor crustal elements, sea salt, and industrial emissions

504   from the UK/western Europe and/or shipping emissions. Factor 2 was also relatively more important

505   from 58.2°N 29.7°W–59.1°N 46.1°W (*geoa*11-15) (Fig. S3, Supplemental Material), i.e. furthest from

506   continental Europe and North America, where local sources such as shipping emissions can contribute

507   relatively more to the TE composition of the bulk aerosol.

508
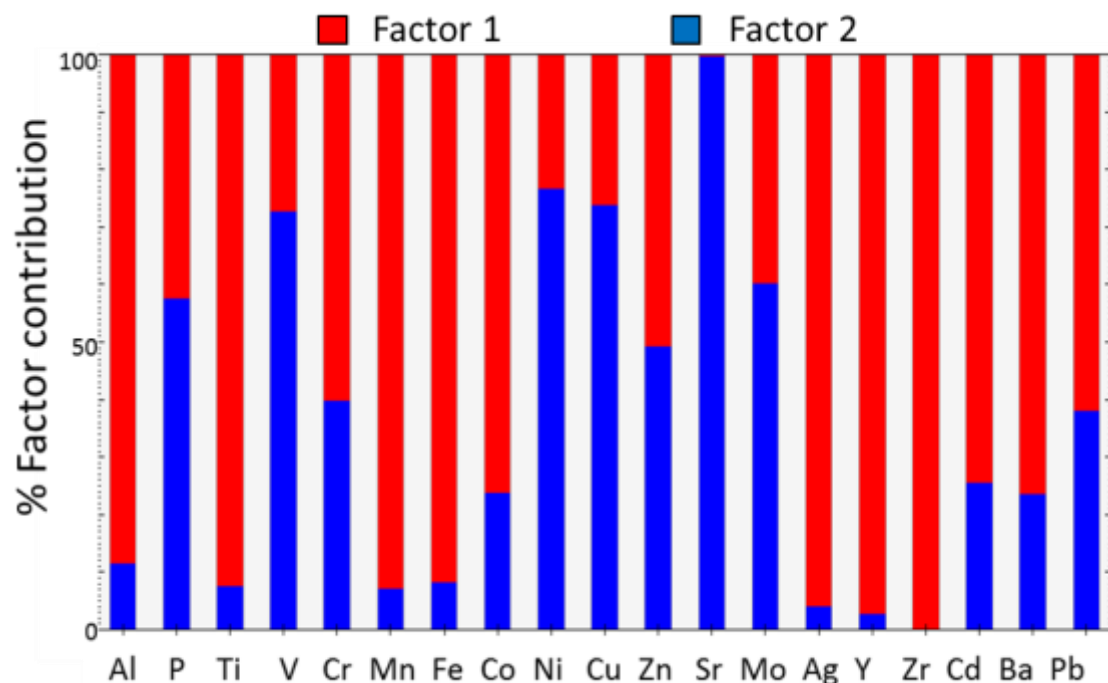
Figure 5. Factor fingerprint of a two factor model of the aerosol samples from *GEOVIDE* for factor

contributions >0.05%. A factor fingerprint is a stacked bar chart which shows the contribution (in

percentage) of each element to the factors.

Rainwater TE distributions

As is often the case at sea, rain events were infrequent during this study (Fig. 6, n = 10), and

tended to occur relatively close to land masses. For example, six of the ten rain events (*geor*1-6)

occurred early in the study at the same location (40.3°N, 10.0°W), over the course of ~36 h (19-20 May

2014). Sample volumes ranged from 13-1100 mL. The sample volume effect (higher concentrations of

TEs observed in smaller sample volumes; Jaffrezo et al., 1990) was tested by fitting an exponential decay

curve to rain samples *geor*1-6 (assumed to be one extended event), but no significant relationship

between sample volume and TE concentrations was observed using this approach (data not shown). As

with the aerosol samples, TE concentrations in rainwater were generally low, with the range in TE

concentrations being comparable to the aerosol concentrations (Fig. 2 and 6). However, in contrast to

the aerosol TE data, the relationship between rainwater Fe and Ti was poor (r^2 = 0.28), suggesting

elemental ratios in rainwater do not reflect crustal ratios. This is likely a result of differences in the

solubility of these TEs, as the rain samples were acidified on collection, but unfiltered.

22
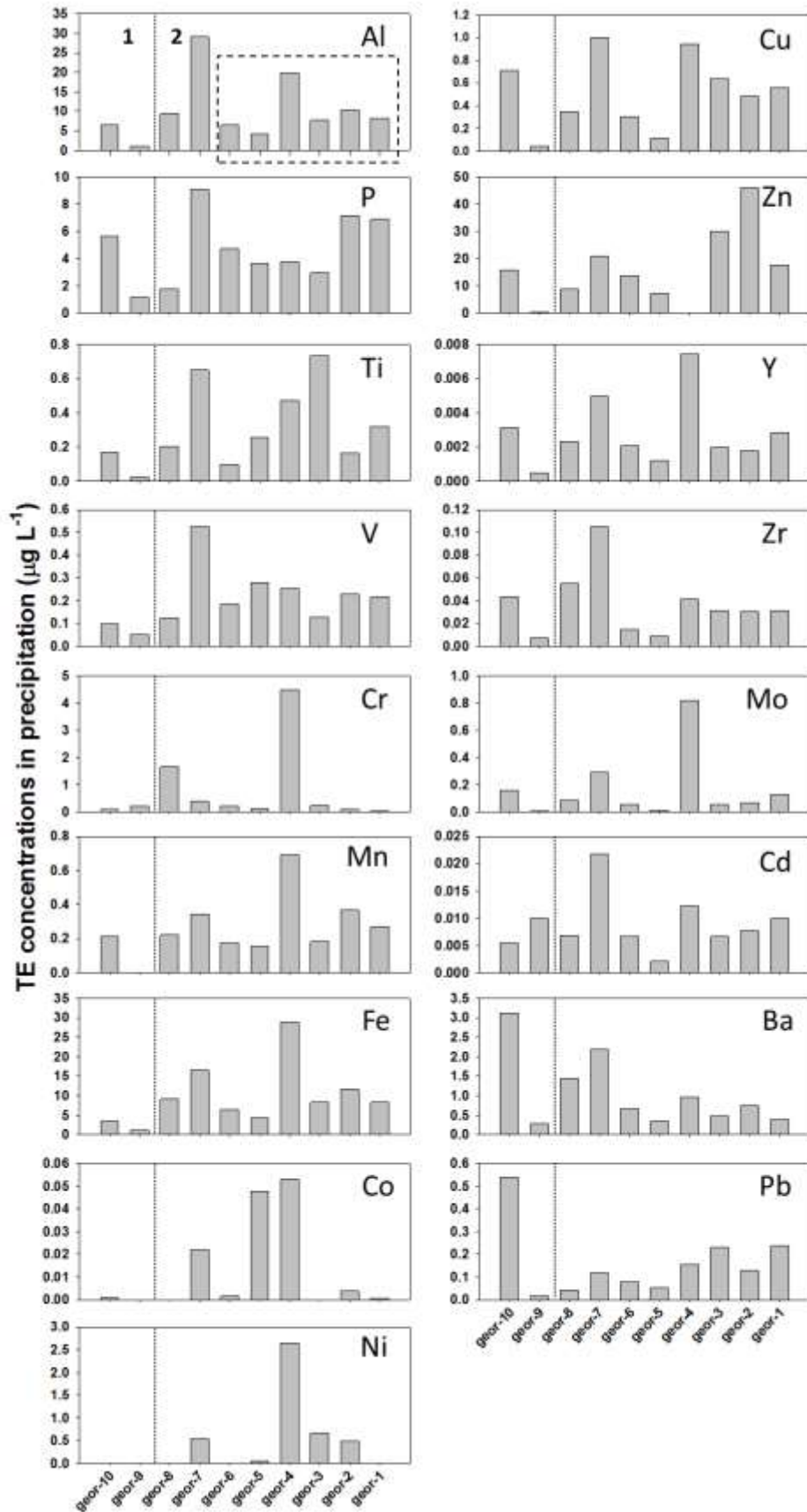
526   Figure 6. Rainwater TE concentrations (µg L^{-1}). The x-axis is reversed to reflect the longitude of the

527   sample locations, i.e., west-east. The dotted line marks the boundary between Areas 1 and 2, and the

528   dashed square surrounds samples *geor*1-6, which were collected in approximately the same location

529   over a 36 h period. The full data set is displayed in Table S2 in the Supplemental Material and has been

530   submitted to the LEFE-CYBER database.

531   <u>Atmospheric deposition fluxes</u>

532   *Dry deposition (traditional approach)*: Marine aerosol samples are collected at sea or from

533   remote island or promontory sites using high or low volume total suspended particulate (TSP) samplers,

534   and dry deposition TE fluxes are estimated from the TE aerosol concentrations multiplied by a dry

535   deposition velocity (V_d; e.g. Duce et al., 1991). The dry deposition fluxes from this study are presented as

536   box and whisker plots to cover the range for each element in the two regions (Areas 1 and 2) either side

537   of 30°W longitude (Fig. 7). As the GEOVIDE aerosol samples were not size-resolved, a V_d of 1.2 cm s^{-1}

538   (Torres-Padrón et al., 2002; Buck et al., 2010) was used for elements with enrichment factors < 10

539   (primarily lithogenic), and 0.3 cm s^{-1} (Chance et al., 2015) for the remaining elements (Cu, Zn, Mo, Ag,

540   Cd, Pb). As TSP samples are only a snapshot of the aerosol composition at that location, taking a boxed

541   approach in this study allows us to estimate a monthly flux (roughly May 2014 for Area 2, and June 2014

542   for Area 1). The median fluxes (indicated by the line in the box plots, Fig. 7) were always higher in Area 2

543   than Area 1 (1.5-11x higher). This was an expected outcome given that the lowest aerosol Ti

544   concentrations, and by implication the lowest aerosol loadings, were observed in Area 1 (Fig. 2). Our dry

545   deposition flux estimates are consistent with those from other low atmospheric deposition regions of

546   the Atlantic Ocean, e.g., 40-68°N (Buck et al., 2010), 40-50°N (Baker et al., 2013), and the southeastern

547   Atlantic (Chance et al., 2015).

548

549

550
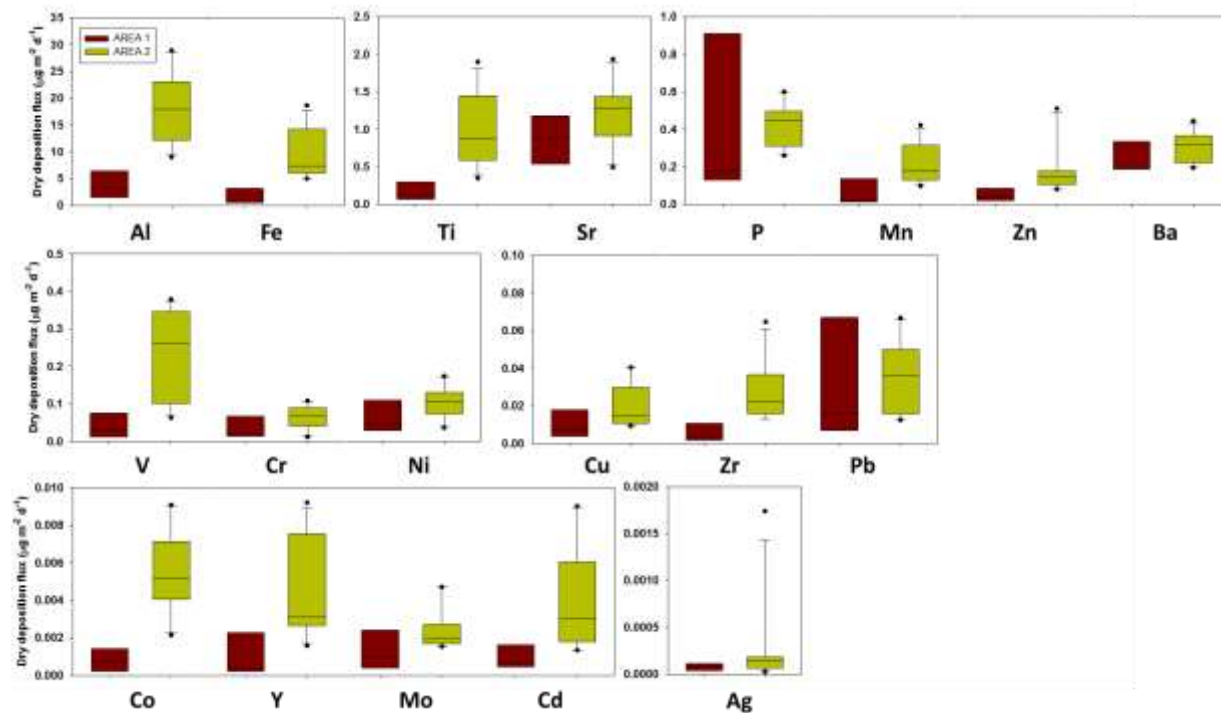
Figure 7. Dry deposition fluxes for Area 1 (red; west of 30°W, n = 7) and Area 2 (green; east of 30°W, n = 11). Note the variable y-axes scales. The horizontal line in the box represents the median value, and the boundaries of the box represent the 25th and 75th percentiles. The error bars (whiskers) indicate the 10th and 90th percentiles. Error bars are not displayed for the Area 1 fluxes as the sample population was too small. All data is given in Table S5 (Supplemental Material).

Wet deposition (traditional approach): Compared to aerosol chemical composition studies, there are relatively few rain water chemical species composition data. The main reason for this is that rain samples are usually collected at sea on an event basis, by fortuitously being in the right place, at the right time. Precipitation sampling has also occurred on remote island or promontory sites, but sampling stations are typically occupied for shorter periods than aerosol sampling sites due to the challenge of sample storage and collection. In addition, there is an ongoing question regarding bias in rainfall measured at land-based sites relative to the surrounding ocean. Furthermore, the location of the sampling site can also introduce bias, for instance, Kadko and Prospero (2011) demonstrated a consistent offset in sampled volumes between samples collected at two locations and altitudes on the island of Bermuda over a two-year period, despite similar meteorological conditions at both sites.

566   In some regions of the open ocean wet deposition exceeds dry deposition (Duce et al., 1991),

567   and even in regions where dry deposition dominates over wet deposition, rain during/after a "dust

568   event" could have important local impacts on TE concentrations in surface waters. For all elements in

569   this study, the wet deposition flux in Area 2 exceeded that in Area 1 by 1-85% (Fig. 8; Table S6). For

570   example, the wet deposition flux estimates for Fe were: 2.3 µg m^{-2} d^{-1} (Area 1) and 26 µg m^{-2} d^{-1} (Area 2),

571   an order of magnitude difference. Given that the median Fe dry deposition flux (assuming a V_d of 1.2 cm

572   s^{-1}) was 0.68 µg m^{-2} d^{-1} for Area 1, and 7.4 µg m^{-2} d^{-1} for Area 2, this data suggests that wet deposition

573   dominated the flux of Fe to our study region during May-June 2014. In regions of the Atlantic Ocean

574   where aerosol supply is not dominated by Saharan dust, the wet and dry deposition fluxes of Fe are

575   thought to be roughly equal (e.g., Chance et al., 2015). In contrast, in areas where Saharan dust

576   represents a significant input (e.g., Bermuda, Sholkovitz et al., 2009) dry deposition dominates. The

577   dominance of the wet deposition flux over the dry flux held for all other TEs in the study area, except Al,

578   P and Ti. In Area 1, wet and dry fluxes were roughly equal, but the wet flux of Ti was only half that of the

579   dry flux. In Area 2, the wet and dry fluxes were roughly equal for these three elements.

580
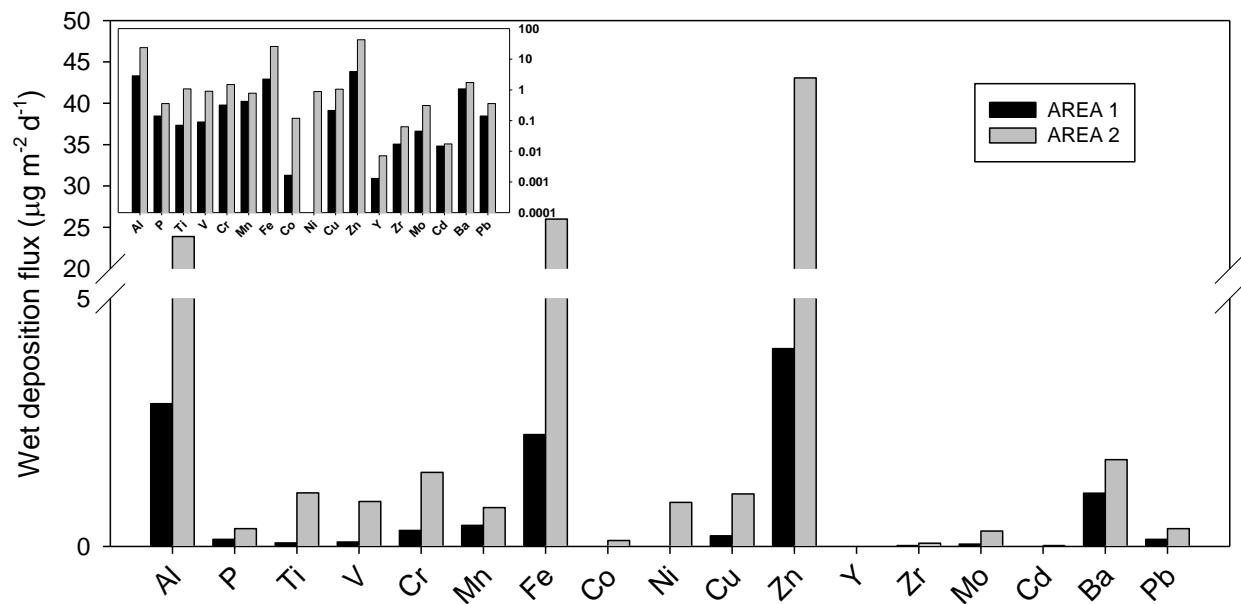
581

582   Figure 8. Wet deposition fluxes for Area 1 (black; west of 30°W) and Area 2 (grey; east of 30°W). Ni was

583   below detection in Area 1. The inset is the same data plotted on a log scale. The data for this plot can be

584   found in Table S6 (Supplemental Material).

585 *Total deposition (^{7}Be approach):*

586   The measured aerosol ^{7}Be concentrations reported in Table 2a (0.078±0.017 – 0.35±0.02 dpm

587   m^{-3}) are comparable with the range of the two years of aerosol ^{7}Be concentration data at Station Alert,

588   Canada (0.0090-0.29 dpm m^{-3}; Dibb et al., 1994), a low-dust regime. However, the true range of ^{7}Be

589   concentrations from this study includes lower concentrations as ^{7}Be activity was below detection in all

590   aerosol samples from the Irminger and Labrador Sea regions (Table S2). This latter point is an important

591   limitation to the use of the ^{7}Be technique, but by increasing the volume of air filtered, and as analytical

592   capabilities improve, an issue that might be expected to occur less frequently.

593

594   Table 2. Concentrations, inventories and deposition flux estimates of ^{7}Be from (a) aerosols, (b) seawater,

595   and (c) bulk deposition (precipitation) samples (± ^{7}Be counting uncertainty). Note that there is no

596   aerosol ^{7}Be data (Table 2a) from 10-23 June 2014 (*geoa*11-16) as ^{7}Be activity was below detection

597   (minimum detectable activity range: 0.019 dpm m^{-3} (*geoa*15) – 0.046 dpm m^{-3} (*geoa*11)) in the Irminger

598   and Labrador Seas. The contribution of dry deposition to total ^{7}Be flux is calculated using the ^{7}Be fluxes

599   derived from aerosol concentrations (Eq. 1) and those derived from the water column inventories (Eq. 5)

600   from the same approximate location (station indicated in brackets). An extended version of this table

601   can be found in the Supplemental Material (Table S3).

602

(a) AEROSOLS					
Area	Sample	Sample date (start)	^{7}Be concentration dpm m^{-3}	Dry ^{7}Be flux dpm m^{-2} d^{-1}	% contribution of dry deposition to total ^{7}Be flux
2	*geoa*1	19-May-14	0.078 ± 0.017	20 ± 5	13 (1)
2	*geoa*2	23-May-14	0.193 ± 0.019	51 ± 5	
2	*geoa*3	24-May-14	0.35 ± 0.02	92 ± 6	65 (13)
2	*geoa*4	25-May-14	0.230 ± 0.012	60 ± 3	42 (13)
2	*geoa*5	27-May-14	0.17 ± 0.03	44 ± 6	
2	*geoa*6	30-May-14	0.088 ± 0.014	23 ± 4	10 (21)
2	*geoa*7	02-Jun-14	0.114 ± 0.011	30 ± 3	
2	*geoa*8	04-Jun-14	0.112 ± 0.012	29 ± 3	
2	*geoa*9	06-Jun-14	0.109 ± 0.018	28 ± 5	9 (32)
2	*geoa*10	08-Jun-14	0.052 ± 0.009	13± 2	
1	*geoa*17	23-Jun-14	0.095 ± 0.011	25 ± 3	19 (69)

| 1 | *geoa*18 | 25-Jun-14 | 0.062 ± 0.009 | 16.0 ± 0.8 | 12 (77) |

			(b) SEAWATER		
			^{7}Be inventory	Total ^{7}Be flux
Area	Station	Sample date	dpm m^{-2}	dpm m^{-2} d^{-1}
2	1	20-May-14	11600 ± 400	151 ± 5
2	13	25-May-14	10900 ± 1100	141 ± 14
2	21	01-Jun-14	17100 ± 600	220 ± 8
2	32	08-Jun-14	23300 ± 800	302 ± 10
2	38	11-Jun-14	10600 ± 900	140 ± 12
1	44	14-Jun-14	5700 ± 1000	74 ± 13
1	60	18-Jun-14	11000 ± 300	143 ± 4
1	69	23-Jun-14	9700 ± 300	126 ± 4
1	77	26-Jun-14	10500 ± 300	136 ± 4

			(c) PRECIPITATION		
		Sample date	^{7}Be concentration	Total ^{7}Be flux
Area	Sample	(start)	dpm m^{-3}	dpm m^{-2} d^{-1}
2	*BeR*-1	17-May-14	87000 ± 3000	484 ± 19
2	*BeR*-2	20-May-14	286000 ± 15000	650 ± 30
2	*BeR*-3	28-May-14	99000 ± 3000	334 ± 11
2	*BeR*-4	05-Jun-14	183000 ± 4000	880 ± 20
1	*BeR*-5	10-Jun-14	64600 ± 1800	354 ± 10
1	*BeR*-6	15-Jun-14	49000 ± 1900	349 ± 13
1	*BeR*-7	23-Jun-14	105000 ± 5000	400 ± 20
1	*BeR*-8	26-Jun-14	111000 ± 8000	255 ± 18

603

604   In this study, dry deposition accounted for 9-65% of the total ^{7}Be deposition flux (Table 2a), the
605 remaining 35-91% being supplied by wet deposition, which is less than the 95% observed during a two-
606 year study on Bermuda by Kadko and Prospero (2011). However, the estimation of the balance of the
607 wet to dry deposition flux is dependent on the deposition velocity used in the dry deposition flux
608 calculation. Here, we used 0.3 cm s^{-1} to represent submicron particles, but the Kadko and Prospero
609 study used 0.1 cm s^{-1}. If we were to have used this lower velocity, then wet deposition would have
610 accounted for 78-97% of the total ^{7}Be flux, which is consistent with the 95% reported for Bermuda.
611 Regardless, these data confirm that wet deposition is the primary mode of delivery for ^{7}Be to surface
612 waters (Young and Silker, 1980).

613   The inventories of ^{7}Be in the water column (Fig. 9) presented in this study (5700-23300 dpm m^{-2})

614   are comparable in magnitude to those reported by Young and Silker (1980) in the North Atlantic for

615   latitudes greater than 40°N (15000-25000 dpm m^{-2}). According to these authors, inventories of ^{7}Be in

616   the North Atlantic are higher in the western part and particularly in the Sargasso Sea region, and lower

617   in the eastern part, particularly in the Canary region. In fact, inventories of ^{7}Be south of 36°N in the

618   Azores-Canary region (15300-30000 dpm m^{-2}, Kadko and Olson 1996) and the Sargasso Sea (24800-

619   50500 dpm m^{-2}, Kadko and Prospero 2011) also show a westward increasing trend. In this study,

620   however, the inventories did not show either south-north or east-west trends. Also, the mean ^{7}Be flux

621   calculated from the water column inventory (160 ± 70 dpm m^{-2} d^{-1}; Table 2b) in this study is 2.9 (± 1.8)

622   times smaller than the mean ^{7}Be flux calculated from precipitation samples (460 ± 210 dpm m^{-2} d^{-1};

623   Table 2c). There are three possible explanations for this mismatch. Firstly, the ^{7}Be fluxes estimated from

624   the precipitation samples integrate over a short time scale (from 1 to 8 days during the cruise), while ^{7}Be

625   fluxes based on the water column inventories integrate on a seasonal time scale (about 2.5 months prior

626   to the sampling date). Therefore, precipitation samples are more sensitive to changes in the variation of

627   surface air concentrations of ^{7}Be compared to the water column inventories, whereby ^{7}Be is

628   homogenised in the mixed layer and relatively insensitive to fluctuations in atmospheric supply (Kadko

629   and Prospero, 2011). Indeed, surface air concentrations of ^{7}Be peak during the warm season as a

630   consequence, in part, of an increased rate of vertical transport within the troposphere, bringing air

631   enriched in ^{7}Be from higher levels to the surface, especially at middle latitudes (Feely et al., 1989). This

632   would explain, at least partially, the higher ^{7}Be fluxes derived from the precipitation samples with

633   respect to those from the water column inventories, since the former only covered warm months

634   (May/June) while the latter also included colder months (from March to May/June). Also, if it had rained

635   less in the preceding few weeks than it did during the *GEOVIDE* campaign the water column inventories

636   would be lower. However, this does not appear to be the case from the satellite data (Figs. S5 and S6,

637   Supplemental Material). Because of the sensitivity of the precipitation data to fluctuations in

638   atmospheric supply of ^{7}Be, and the time of year of this study, the inventory of ^{7}Be in the upper water

639   column is the preferred choice for calculating ^{7}Be-derived TE fluxes on a seasonal time scale. Secondly,

640   ^{7}Be can be scavenged by particles in coastal environments (e.g., Sommerfield et al., 1999; Venti et al.,

641   2012). Here, in the open ocean, which is characterised by low particle regimes, we assumed that this

642   would be negligible, in accord with the pioneering work of Kadko et al. (2015; 2016). However, we note

643   that phytoplankton blooms were observed at some locations during the cruise. Therefore, the

644   discrepancy may also be a result of the scavenging of ^{7}Be to suspended particles and subsequent sinking

645   to depth. Given that a steady state flux is needed to sustain the seawater inventories shown in Table 2b,

646   and that scavenging of Be by sinking particles is sensitive to the composition of the particles (Chase et

647   al., 2002; Chuang et al., 2015), constraining loss of ^{7}Be via particle scavenging and export deserves

648   further investigation, especially in regions where intense phytoplankton blooms occur. Finally, upwelling

649   of ^{7}Be-poor waters can replace ^{7}Be-rich surface waters. Upwelling is favoured by northerly winds,

650   typically from April to September, off the coast off Portugal (Lemos and Pires, 2004). The distribution of

651   temperature and density in the water column off Lisbon did not reveal strong upwelling events during

652   the study. However, because northerly winds were dominant 2-3 months before sampling, some

653   underestimation of the water column inventory of ^{7}Be cannot be ruled out at stations 1 and 13.

654   Consequently, considering the potential effects of scavenging and upwelling, we note that the water

655   column inventories presented in this study provide conservative estimations for the atmospheric fluxes

656   of ^{7}Be, and hence TEs.

657
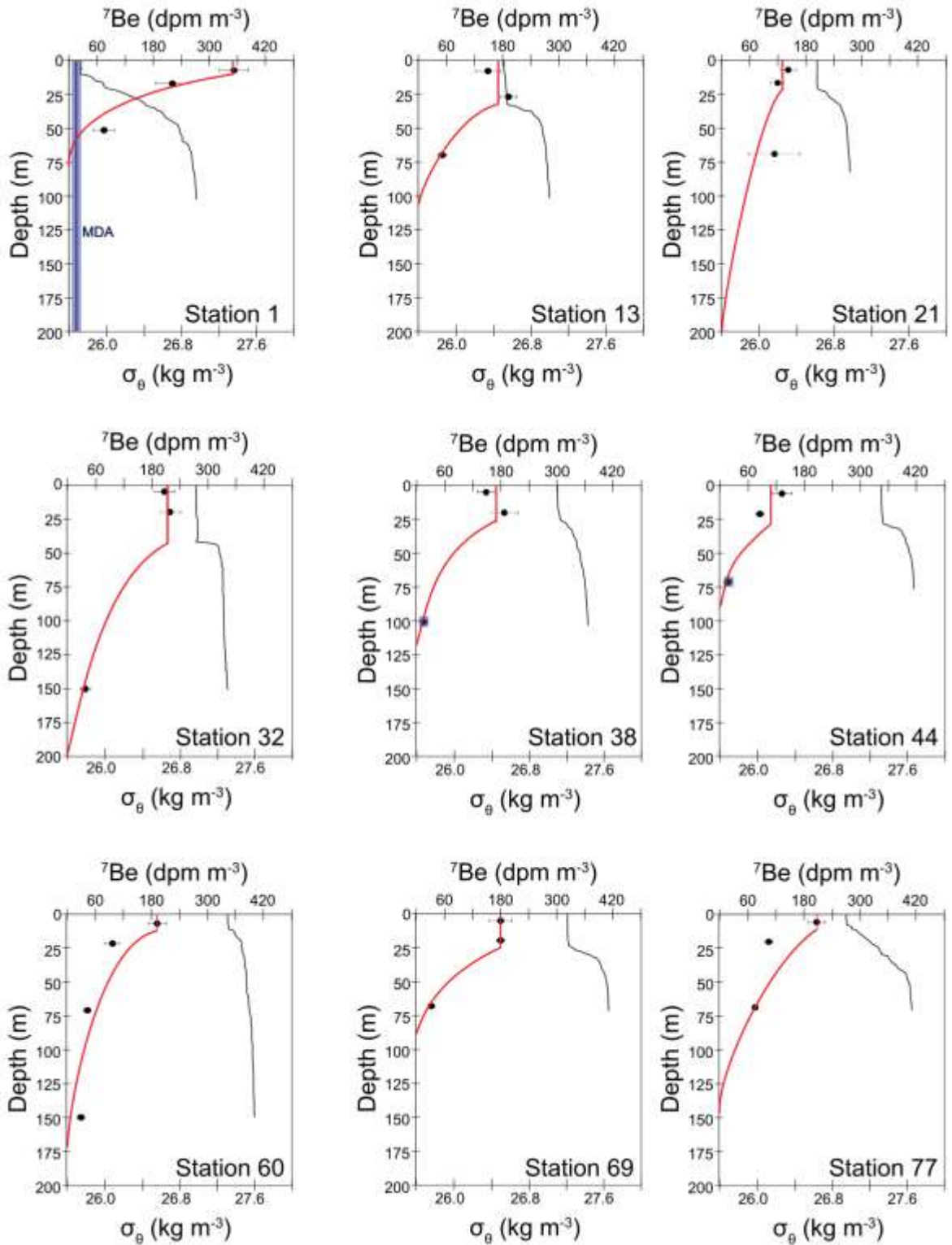
Figure 9. Concentration profiles (black dots), integrated inventory of [7]Be (red continuous line) in the
water column and potential density anomaly (σ_θ, black continuous line) for all stations sampled during
the GEOVIDE cruise. The Minimum Detectable Activity (MDA) averaged from all [7]Be measurements

661 (19±8 dpm m^{-3}) is shown in the panel for Station 1 (shaded blue area). The inventory of ^{7}Be below the

662 mixed layer was calculated using a simple exponential fitting taking into account the concentrations of

663 ^{7}Be at the base of the mixed layer and below. Depths where the fitting-derived ^{7}Be concentration would

664 be 1% of that in the mixed layer are: 77 m (station 1), 106 m (station 13), 199 m (station 21), 211 m

665 (station 32), 116 m (station 38), 83 m (station 44), 167 m (station 60), 94 m (station 69) and 151 m

666 (station 77). For the exponential fitting, average MDA values were assigned to concentrations of ^{7}Be

667 below the MDA found at station 38 (100 m) and station 44 (70 m). At station 21, the exponential fitting

668 led to a clear overestimation of the inventory and predicted the presence of ^{7}Be far below (up to 9000

669 m) the bottom depth at that station (4467 m). Because this approach led to unreasonable inventories, a

670 new exponential fitting with a fixed slope (averaged from the slopes of the other stations) was used.

671

672 Comparison of flux estimates

673   In order to assess how total (i.e., dry plus wet) atmospheric fluxes calculated using the

674 traditional approach (Eqs 1 and 2), and using the ^{7}Be method (Eq. 7) compare for the species of interest,

675 the data is plotted for Areas 1 and 2 (Fig. 10).

676
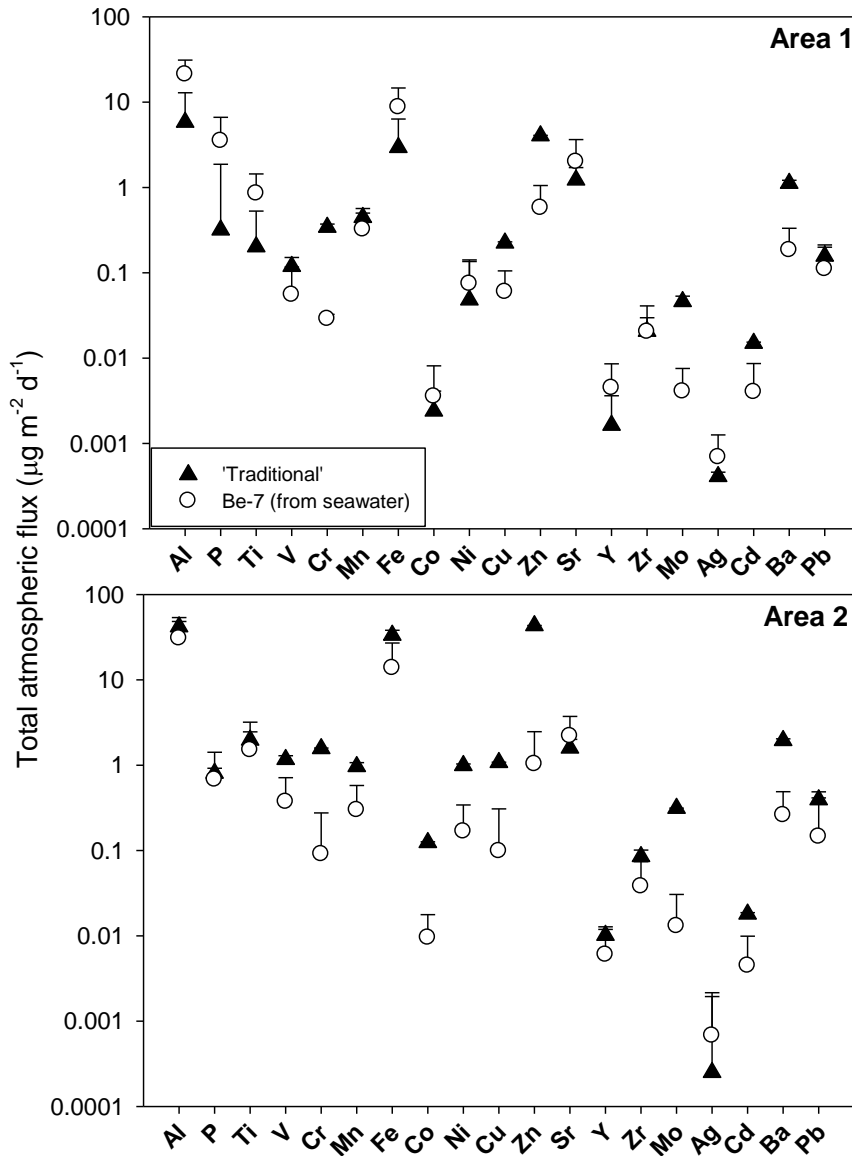
Figure 10. Comparison of the median TE fluxes (+ 1 SD) calculated using dry + wet deposition estimates (traditional approach, black triangles), and the [7]Be approach using the [7]Be inventory in seawater (open circles). Only positive error bars are displayed because negative values cannot be plotted on a log scale. Negative values occur when the SD is greater than the median value. The data for these plots can be found in Table S7 (Supplemental Material).

In Area 1 there was very good agreement for V, Mn, Co, Ni, Sr, Zr and Pb (median values within one positive SD of the lower value). For Cr, Cu, Zn, Mo, Cd and Ba the traditional approach resulted in estimates 3.5-12 times higher. In contrast, for Al, P, Ti, Fe, Y and Ag the [7]Be approach resulted in estimates from 2-11 times higher. In Area 2 there was very good agreement between flux estimates for

686   Al, P, Ti, Sr, Y, Zr, Ag and Pb, whereas the traditional approach resulted in flux estimates 2-42 times

687   higher for V, Cr, Mn, Fe, Co, Cu, Ni, Zn, Mo, Cd and Ba. There are a couple of points that should be

688   noted. Firstly, the TEs with good agreement between the flux estimates were not the same in the two

689   areas. This could simply be the result of the disparity between the number of samples in each area (only

690   2 for Area 1, compared to 10 for Area 2), or there could be systematic differences in how TEs are

691   delivered to the surface ocean and their subsequent behaviour in the water column following

692   deposition. Secondly, the traditional approach results in higher median estimates for all TEs (except Ag

693   and Sr) in Area 2 and for six TEs (Cr, Cu, Zn, Mo, Cd and Ba) in Area 1, whereas the [7]Be approach yielded

694   higher estimates for a number of lithogenic TEs in Area 1. The possible reasons for this offset are

695   explored and suggestions made for future studies applying these techniques for TE deposition flux

696   estimation.

697   (i) The two techniques provide estimates on different timescales: The traditional approach

698   provides a snap shot of deposition (and aerosol TE concentrations show significant day-to-day

699   variability), whereas the [7]Be technique provides a seasonal estimate for spring (March-April-May-June)

700   2014. As the inventory of [7]Be is a reflection of the mean life-time of [7]Be in the water column, and [7]Be

701   deposition is lowest in the cooler months prior to the cruise (Young and Silker, 1980; Akata et al., 2008),

702   the [7]Be inventories used here most likely encompassed a period of time when [7]Be atmospheric inputs

703   were lower than at the time of our field campaign. The impact of the different timescales of integration

704   are best exemplified by the higher [7]Be flux estimates derived from precipitation samples compared with

705   the water column inventories. The higher TE flux estimates derived from the traditional approach in

706   several instances, particularly in Area 2, could also be directly related to this temporal mismatch, with

707   aerosol samples representing up to 48 h integrations and the water column inventory, approximately

708   2.5 months. This is highly relevant for constraining atmospheric deposition on seasonal, or annual,

709   timescales in models.

710   (ii) Representative dry deposition velocities: Aerosol TEs released by high temperature industrial

711   processes tend to be smaller than lithogenic and sea salt aerosols and, thus, have a smaller V_d (Duce et

712   al. 1991). The uncertainties that the V_d term introduces to the dry deposition flux estimates provide the

713   impetus to find new ways to constrain this term. Constraint of this term requires accurate

714   parameterisation of wind speed, relative humidity and particle type (Slinn and Slinn, 1981). As we do not

715   have data describing the particle size distribution and type for this study, it is challenging to constrain

716   the uncertainties, but it is proposed to be up to a factor of three (Duce et al., 1991). Although we cannot

717 verify the validity of this uncertainty, we can calculate an effective bulk deposition velocity (combined

718 dry and wet aerosol deposition velocity; Table 3) from Equation 5 (Kadko et al., 2016), and use it to

719 suggest where wet deposition is likely to be an important factor for the delivery of TEs, and/or where

720 there may be an unaccounted loss term for [7]Be (e.g., scavenging in the water column). It should be

721 noted that this approach assumes that a fixed deposition velocity of 1000 m d^{-1} (Duce et al., 1991; Buck

722 et al., 2010) is appropriate for mineral dust deposition in the remote North Atlantic.

723 Table 3. The effective bulk deposition velocity (± propagated uncertainty) calculated using the [7]Be fluxes

724 derived from seawater and aerosol concentrations of [7]Be (using Eq. 5) from samples collected at the

725 same approximate location. Note that there is no data for samples *geo*a11-16, inclusive, as [7]Be was

726 below detection in aerosol samples at the time of station occupation.

Area	Aerosol sample	Water column station	Bulk V_d	
			m d^{-1}	cm s^{-1}
2	geoa1	1	1900 ± 400	2.2 ± 0.5
2	geoa4	13	610 ± 70	0.71 ± 0.08
2	geoa6	21	2500 ± 400	2.9 ± 0.5
2	geoa9	32	2800 ± 500	3.2 ± 0.6
1	geoa17	69	1330 ± 160	1.54 ± 0.18
1	geoa18	77	2200 ± 300	2.6 ± 0.4
2	Mean (±1 SD)		2000 ± 1000	2.3 ± 1.1
1	Mean (±1 SD)		1800 ± 600	2.0 ± 0.7
1+2	Mean (±1 SD)		1900 ± 800	2.2 ± 0.9

727

728   Where the bulk deposition velocities displayed in Table 3 are significantly greater than 1000 m d^{-}

729 ^{1}, it suggests that wet deposition played a significant role in determining the total TE fluxes, as

730 demonstrated by the calculated wet and dry deposition fluxes (Figs. 7 and 8). With the exception of

731 sample *geo*a4 (Station 13), this was the case throughout the cruise. While rain events were infrequently

732 sampled, humidity was generally >90% and thick fog was frequently encountered between 27 May 2014

733 (*geo*a5) and 25 June 2014 (*geo*a17). Values close to or less than 1000 m d^{-1} suggest that there is a loss

734 term missing from our equations, or that the aerosol size distribution was dominated by fine mode, sub-

735 micron particles with lower dry deposition velocities. However, as internal mixing with sea salt aerosols

736 leads to some degree of homogenisation in the size distribution of remote marine aerosols (Andreae et

737 al., 1986) this explanation is doubtful, but could be tested with a size-resolved aerosol sampling

738 strategy.

739   (iii) The assumption of negligible scavenging of [7]Be onto sinking particles may be incorrect:

740   Bearing in mind that the study region is an area subject to intense phytoplankton blooms during spring

741   (the season of the present study), and that Be has an affinity for a variety of particle types (Chase et al.,

742   2002; Chuang et al., 2015), neglecting this term may result in an underestimation of the TE fluxes using

743   the [7]Be approach. Indeed, the effective bulk deposition calculations suggest that for some stations water

744   column scavenging of [7]Be could have been significant. Particle scavenging during this study will be the

745   subject of a separate manuscript (N. Lemaitre et al., in prep), and future studies using the [7]Be approach

746   should aim to quantify and parameterise scavenging of [7]Be onto sinking particles.

747   (iv) Representative precipitation rates: The precipitation rate term is the largest source of

748   uncertainty in wet deposition flux calculations, as it can be challenging to determine accurate values in

749   remote marine regions (e.g., Chance et al., 2015). In this study, the precipitation rates used were based

750   on averages retrieved from satellite products (TRMM and GPM from Giovanni). Precipitation rates

751   determined from field sampling can be inaccurate due to the confounding influence of sea spray,

752   variable wind speeds and no splash screens on the samplers, and in some regions (although not

753   applicable to this study), evaporation. As such the parameterisation of precipitation rate most certainly

754   introduced errors to the calculation of the dry + wet flux (black triangles in Fig. 10). We are reluctant to

755   quantify this uncertainty without having explicitly tested for it. However, by comparing the precipitation

756   rate of 2 mm d^{-1} used for the wet flux calculations with the range of precipitation rates determined from

757   field collections (2 -7 mm d^{-1}) we hypothesise that an error of three to fourfold is not unreasonable. For

758   the [7]Be approach the issue of precipitation rate is avoided by using the [7]Be inventory in seawater rather

759   than [7]Be concentrations from precipitation samples, as the former is less impacted by short-term

760   fluctuations in [7]Be inputs.

761   In reality, a combination of several, or all, of the above points likely contributes to the variability

762   in the TE flux estimates. The motivation for making comparisons between these two approaches for TE

763   flux estimation is driven by the knowledge that one of the biggest challenges currently faced in aerosol

764   studies is converting aerosol chemical concentration data into realistic flux estimates (Anderson et al.,

765   2016). From this study we are confident that [7]Be can be successfully used as a tracer of the atmospheric

766   flux of TEs to the surface ocean in diverse oceanographic settings, particularly where precipitation

767   sampling is either not possible, or is unlikely to be representative. However, effective bulk deposition

768   velocities ≤1000 m d^{-1} suggest that there could be regions where the [7]Be approach should be used with

769   caution, such as in particulate-rich open ocean regimes. As such, it would be advisable to continue to

36

770   test the underlying assumptions of the ^{7}Be approach in order to reduce uncertainties in the deposition

771   flux estimates.

772   **CONCLUSIONS**

773   Atmospheric deposition of TEs to the study region was low throughout May-June 2014, and

774   particularly low in the Irminger and Labrador Seas, as suggested by the aerosol Ti concentrations (range:

775   0.0084-1.9 ng m^{-3}). Despite the cruise track of *GEOVIDE* being located north of the extent of the Saharan

776   dust plume, the positive matrix factorisation (PMF) output indicated that the data could be reduced to

777   only two factors, suggesting that the aerosol TE composition could be represented as simply the mixing

778   of two aerosol sources (1 = mineral dust, and 2 = mixed mineral dust-sea salt-anthropogenic aerosols),

779   largely controlled by the proximity to major land masses.

780   Trace element deposition fluxes (in particular, Fe) are a key component of ocean

781   biogeochemical models, due to the link between TE supply and the biological carbon pump, yet remain

782   poorly constrained as flux estimates are subject to relatively large uncertainties. Here, we investigated

783   the use of ^{7}Be as a tracer of atmospheric inputs. The TE flux estimates obtained by using the ^{7}Be proxy

784   and the traditional approach (dry + wet deposition) were in excellent agreement for approximately half

785   the TEs investigated, but there were large offsets for other TEs (up to 40x). While our results suggest

786   that the ^{7}Be approach continues to show promise in this application, particularly in regions where

787   precipitation samples cannot be routinely collected, it is important to consider factors such as the

788   timescale of integration, selection of representative deposition velocities and precipitation rates, and

789   particle scavenging and export of ^{7}Be from the mixed layer. As such, the underlying assumptions of the

790   ^{7}Be approach should be examined closely to assess their validity in the region of interest. Work

791   continues to this end. In the meantime, our data provide seasonal TE deposition fluxes for the key

792   *GEOTRACES* elements, and more, for the North Atlantic Ocean (>40°N) that can be used to help

793   constrain aerosol TE deposition models.

794

810

811   **REFERENCES**

812   Akata, N., Kawabata, H., Hasegawa, H., Sato, T., Chikuchi, Y., Kondo, K., Hisamatsu, S., and Inaba, J.,
813   2008. Total deposition velocities and scavenging ratios of 7be and 210Pb at Rokkasho, Japan. Journal of
814   Radioanalytical and Nuclear Chemistry, 277, 347-355.

815   Anderson, R.F., Cheng, H., Edwards, R., L., Fleisher, M.Q., Hayes, C.T., Huang, K.F., Kadko, D., Lam, P.J.,
816   Landing, W.M., Lao, Y., Lu, Y., Measures, C.I., Morton, P.L., Moran, S.B., Robinson, L.F., and Shelley, R.U.
817   (2016). How well do we quantify dust deposition to the ocean? Phil. Transact. Royal Soc. A. Doi:
818   10.1098/rsta.2015.0285.

819   Andreae, M.O., Charlson, R.J., Bruynseels, F., Storms, H., van Grieken, R., and Maenhaut, W., 1986.
820   Internal mixture of sea salt, silicates, and excess sulfate in marine aerosols. Science. 232: 1620-1623.

821   Baker, A.R., and, Croot, P.L., 2010. Atmospheric and marine controls on aerosol iron solubility in
822   seawater. Mar. Chem. 120, 4-13.

823   Baker, A.R. and Jickells, T.D., Atmospheric deposition of soluble trace elements along the Atlantic
824   Meridional Transect (AMT). Submitted to Prog. Oceanogr.

825   Baker, A. R., Adams, C., Bell, T.G., Jickells, T.D., and Ganzeveld, L., 2013. Estimation of atmospheric
826   nutrient inputs to the Atlantic Ocean from 50N to 50S based on large-scale filed sampling: Iron and
827   other dust-associated elements, Global Biogeochem. Cycles. 27, 755-767.

828   Baker, A. R., Jickells, T. D., Biswas, K. F., Weston, K., and French, M., 2006. Nutrients in atmospheric
829   aerosol particles along the Atlantic Meridional Transect. Deep Sea Res. Pt II. 53, 1706-1719.

830   Baker, A. R., Lesworth, T., Adams, C., Jickells, T. D., and Ganzeveld, L., 2010. Estimation of atmospheric
831   nutrient inputs to the Atlantic Ocean from 50°N to 50°S based on large-scale field sampling: Fixed
832   nitrogen and dry deposition of phosphorus, Global Biogeochem Cycles. 24. Doi: 10.1029/2009gb003634.

833   Buck, C. S., Landing, W.M., Resing, J.A. and Measures, C.I., 2010. The solubility and deposition of aerosol
834   Fe and other trace elements in the North Atlantic Ocean: Observations from the A16N CLIVAR/CO$_2$
835   repeat hydrography section. Mar. Chem. 120, 57-70.

836   Cámara-Mor, P., Masque, P., Garcia-Orellana, J., Kern, S., Cochran, J. K., and Hanfland, C. 2011.
837   Interception of atmospheric fluxes by Arctic sea ice: Evidence from cosmogenic ^{7}Be. J. Geophys. Res.
838   Oceans. 116, 1–10. Doi: 10.1029/2010JC006847.

839   Celo, V., Dabek-Zlotorzynska, E., and McCurdy, M. 2015. Chemical characterization of exhaust emissions
840   from selected Canadian marine vessels: the case of trace metals and lanthanoids. Env. Sci. Technol. 49,
841   5220-5226.

842   Chance, R., Jickells, T.D., and Baker, A.R., 2015. Atmospheric trace metal concentrations, solubility and
843   deposition fluxes in remote marine air over the south-east Atlantic. Mar. Chem. 177, 45-56. Doi:
844   10.1016/j.marchem.2015.06.028.

845   Chase, Z., Anderson, R.F., Fleisher, M.Q., and Kubik, P.W., 2002. The influence of particle composition
846   and particle flux on scavenging of Th, Pa and Be in the ocean. Earth Planet. Sci. Lett. 204, 215-229.

847   Cheize, M., Sarthou, G., Croot, P., Bucciarelli, E., Baudoux, A.-C., and Baker, A., 2012. Iron organic
848   speciation determination in rainwater using cathodic stripping voltammetry. Anal. Chim. Acta. 726, 45-
849   54.

850   Chuang, C.-Y., Santschi, P.H., Xu, C., Jiang, Y., Ho, Y.-F., Quigg, A., Guo, L., Hatcher, P.G., Ayranov, M., and
851   Schumann, D., 2015. Molecular level characterization of diatom-associated biopolymers that bind ^{234}Th,
852   ^{233}Pa, ^{210}Pb, and ^{7}Be in seawater: A case study with Phaeodactylum tricornutum. J. Geophys Res.
853   Biogeosci. 120, 1858-1869.

854   Comero, S., Gawlik, B.M., and Capitani, L. 2009. Positive Matrix Factorisation (PMF): an introduction to
855   the chemometric evaluation of environmental monitoring data using PMF. JRC scientific and technical
856   reports. Available at: http://publications.jrc.ec.europa.eu/repository/bitstream/JRC52754/reqno_
857   jrc52754_final_pdf_version%5B1%5D.pdf, (accessed 24/03/2016).

858   d'Almeida, G. A., 1986. A model for Saharan dust transport. J. Clim. Appl. Meteorol. 24, 903–916.

859   Dammshäuser, A., Wagener, T., Garbe-Schönberg, D., and Croot, P.L. 2013. Particulate and dissolved
860   aluminum and titanium in the upper water column of the Atlantic Ocean. Deep Sea Res. Pt I. 73, 127-
861   139.

862   de Leeuw, G., Andreas, E.L., Anguelova, M.D., Fairall, C. W., Lewis, E.R., O'Dowd, C., and Schulz, M.,
863   2011. Production flux of sea spray aerosol. Rev. Geophys. 49. Doi: 10.1029/2010RG000349.

864   de Villiers, S. 1999. Seawater strontium and Sr/Ca variability in the Atlantic and Pacific oceans. Earth
865   Planet. Sci. Lett. 171, 623-634.

866   Dibb, J. E., Meeker, L.D., Finkel, R.C., Southon, J.R., Caffee, M.W., 1994. Estimation of stratospheric input
867   to the Arctic troposphere: [7]Be and [10]Be in aerosols at Alert, Canada. J. Geophys. Res. 99, 12855-12864.

868   Doherty, O. M., Riemer, N., and Hameed, S. 2012. Control of Saharan mineral dust transport to Barbados
869   in winter by the Intertropical Convergence Zone over West Africa. J. Geophys. Res. Atmos. 117. Doi:
870   10.1029/2012JD017767.

871   Duce, R. A., Liss, P. S., Merrill, J. T., Atlas, E. L., Buat-Menard, P., Hicks, B. B., Miller, J. M., Prospero, J. M.,
872   Arimoto, R., Church, T. M., Ellis, W., Galloway, J. N., Hansen, L., Jickells, T. D., Knap, A. H., Reinhardt, K.
873   H., Schneider, B., Soudine, A., Tokos, J. J., Tsunogai, S., Wollast, R., and Zhou, M., 1991. The atmospheric
874   input of trace species to the world ocean, Global Biogeochem. Cycles. 5, 193-259.

875   Feely, H. W., Larsen, R.J., and Sanderson, C.G. 1989. Factors that cause seasonal variations in Beryllium-7
876   concentrations in surface air. J. Env. Radioact. 9, 223-249.

877   Ganzeveld, L., Lelieveld, J., and Roelofs, G.-J. 1998. A dry deposition parameterization for sulfur oxides in
878   a chemistry and general circulation model. J. Geophys. Res. Atmos. 103, 5679-5694.

879   Gelado-Caballero, M. D., López-García, P., Prieto, S., Patey, M.D., Collado, C., Hérnández-Brito, J.J., 2012.
880   Long-term aerosol measurements in Gran Canaria, Canary Islands: Particle concentration, sources and
881   elemental composition. J. Geophys. Res. Atmos. 117. Doi: 10.1029/2011jd016646.

882   Jaffrezo, J. L., Colin, J. L., and Gros, J. M., 1990. Some physical factors influencing scavenging ratios.
883   Atmos. Environ. A-Gen. 24, 3073–3083. Doi: 10.1016/0960-1686(90)90486-7.

884   Jickells, T. D., An, Z.S., Andersen, K.K., Baker, A.R., Bergametti, G., Brooks, N., Cao, J.J., Boyd, P.W., Duce,
885   R.A., Hunter, K.A., Kawahata, H., Kubilay, N., laRoche, J., Liss, P.J., Mahowald, N., Prospero, J.M.,
886   Ridgwell, A.J., Tegen, I., and Torres, R., 2005. Global iron connections between desert dust, ocean
887   biogeochemistry and climate. Science, 308, 67-71.

888   Jickells, T. D., and Spokes, L., 2001. Atmospheric iron inputs to the ocean, in The Biogeochemistry of Iron
889   in Seawater, edited by D.A. Turner and K.A. Hunter, pp. 85–121, Hoboken, N. J.: John Wiley.

890   Kadko, D., and Olson, D., 1996. Be-7 as a tracer of surface water subduction and mixed layer history.
891   Deep Sea Res. 43, 89-116.

892   Kadko, D., and Prospero, J.P., 2011. Deposition of [7]Be to Bermuda and the regional ocean:
893   Environmental factors affecting estimates of atmospheric flux to the ocean. J. Geophys. Res. 116. Doi:
894   10.1029/2010JC006629.

895   Kadko, D., Galfond, B., Landing, W.M., and Shelley, R.U. 2016. Determining the pathways, fate and flux
896   of atmospherically derived trace elements in the Arctic Ocean/ Ice system. Mar. Chem. 182, 38-50.

897   Kadko, D., Landing, W.M., and Shelley, R.U., 2015. A novel tracer technique to quantify the atmospheric
898   flux of trace elements to remote ocean regions. J. Geophys. Res. Oceans. Doi: 10.1002/2014JC010314.

899 Law, C. S., Breviere, E., de Leeuw, G., Garcon, V., Guieu, C., Kieber, D.J., Kontradowitz, S., Paulmier, A.,
900 Quinn, P.K., Saltzman, E.S., Stefels, J., and von Glasow, R., 2013. Evolving research directions in Surface
901 Ocean-Lower Atmosphere (SOLAS) science. Environ. Chem. 10, 1-16.

902 Lemos, R.T., and Pires, H.O., 2004. The upwelling regime off the west portuguese coast, 1941-2000. Int.
903 J. Climatol. 24, 511–524.

904 Monterey, G., and Levitus, S., 1997. Seasonal variability of mixed layer depth for the world ocean. NOAA
905 Atlas, NESDIS, 14, Washington, D.C., 96 pp.

906 Moore, C. M., Mills, M. M., Arrigo, K. R., Berman-Frank, I., Bopp, L., Boyd, P. W., Galbraith, E. D., Geider,
907 R. J., Guieu, C., Jaccard, S. L., Jickells, T. D., La Roche, J., Lenton, T. M., Mahowald, N. M., Maranon, E.,
908 Marinov, I., Moore, J. K., Nakatsuka, T., Oschlies, A., Saito, M. A., Thingstad, T. F., Tsuda, A., and Ulloa,
909 O., 2013. Processes and patterns of oceanic nutrient limitation. Nature Geosci. 6, 701-710.

910 Morel, F. M. M., and Price, N.M., 2003. The biogeochemical cycles of trace metals in the oceans Science.
911 300, 944-947.

912 Morton, P. L., Landing, W.M., Hsu, S.-C., Milne, A., Aguilar-Islas, A.M., Baker, A.R., Bowie, A.R., Buck, C.S.,
913 Gao, Y., Gichuki, S., Hastings, M.G., Hatta, M., Johansen, A. M., Losno, R., Mead, C., Patey, M.D., Swarr,
914 G., Vandermark, A., Zamora, L.M., 2013. Methods for the sampling and analysis of marine aerosols:
915 results from the 2008 GEOTRACES aerosol intercalibration experiment. Limnol. Oceanogr. Methods. 11,
916 62-78.

917 Moulin, C., Lambert, C.E., Dulac, F., and Dayan, U., 1997. Control of atmospheric export of dust from
918 North Africa by the North Atlantic Oscillation. Nature. 387, 691-694.

919 Nair, P. R., Parameswaran, K., Abraham, A., and Jacob, S. 2005. Wind-dependence of sea-salt and non-
920 sea-salt aerosols over the oceanic environment. J. Atmos. Solar-Terr. Phys. 67, 884-898.

921 Pacyna, J.M., and Pacyna, E.G., 2001. An assessment of global and regional emissions of trace metals to
922 the atmosphere from anthropogenic sources worldwide. Environ. Rev. 9: 269-298.

923 Prospero, J. M., and Carlson, T.N., 1972. Vertical and areal distribution of Saharan dust over the
924 Equatorial North Atlantic Ocean. J. Geophys. Res. 77, 5255-5265.

925 Prospero, J. M., Collard, F.-X., Molinie, J., and Jeannot, A., 2014. Characterizing the annual cycle of
926 African dust transport to the Caribbean Basin and South America and its impact on the environment and
927 air quality. Global Biogeochem. Cycles. 29, 757-773.

928 Rolph, G.D., 2016. Real-time Environmental Applications and Display sYstem (READY). Website
929 (http://ready.arl.noaa.gov). NOAA Air Resources Laboratory, Silver Spring, MD.

930 Rudnick, R.L., and Gao, S., 2003. Composition of the continental crust. In: H.D. Holland, and Turekian,
931 K.K. (Editor), Treatise on Geochemistry. Elsevier, Oxford, pp. 1-64.

932 Saito, M. A., Goepfert, T.J., Ritt, J.T., 2008. Some thoughts on the concept of colimitation: Three
933 definitions and the importance of bioavailability. Limnol. Oceanogr. 53, 276-290.

934 Schlosser, C., Klar, J.K., Wake, B.D., Snow, J.T., Honey, D.J., Woodward, E.M.S., Lohan, M.C., Achterberg,
935 E.A., and Moore, C.M., 2013. Seasonal ITCZ migration dynamically controls the location of the
936 (sub)tropical Atlantic biogeochemical divide. PNAS. Doi: 10.1073/pnas.1318670111.

937 Shelley, R. U., Morton, P.L., and Landing, W.M., 2015. Elemental ratios and enrichment factors in
938 aerosols from the US-*GEOTRACES* North Atlantic transects. Deep Sea Res. Pt II. 116, 262-272.

939 Sholkovitz, E., R., Sedwick, P.N. and Church, T.M., 2009. Influence of anthropogenic combustion
940 emissions on the deposition of soluble aerosol iron to the ocean: Empirical estimates for island sites in
941 the North Atlantic. Geochim. Cosmochim. Acta. 73, 3981-4003.

942 Sieck, L. C., Burges, S. J., and Steiner, M., 2007. Challenges in obtaining reliable measurements of point
943 rainfall. Water Resour. Res. 43. Doi: 10.1029/2005WR004519.

944 Silker, W. B., 197. Beryllium-7 and fission products in the Geosecs II water column and applications of
945 their oceanic distributions. Earth Plan. Sci Lett. 16, 131-137.

946 Slinn, S. A., and Slinn, W.G.N., 1981. Predictions for particle deposition on natural waters. Atmos.
947 Environ. 14, 1013-1016.

948 Sommerfield, C.K., Nittrouer, C.A., Alexander, C.R., 1999. ^{7}Be as a tracer of flood sedimentation on the
949 northern California continental margin. Cont. Shelf Res. 19, 335–361. Doi:10.1016/S0278-
950 4343(98)00090-9.

951 Stein, A.F., Draxler, R.R, Rolph, G.D., Stunder, B.J.B., Cohen, M.D., and Ngan, F., 2015. NOAA's HYSPLIT
952 atmospheric transport and dispersion modeling system. Bull. Amer. Meteor. Soc. 96, 2059-2077,
953 http://dx.doi.org/10.1175/BAMS-D-14-00110.1.

954 Streibel, T., Schnelle-Kreis, J., Czech, H., Harndorf, H., Jakobi, G., Jokiniemi, J., Karg, E., Lintelmann, J.,
955 Matuschek, G., Michalke, B., Müller, L., Orasche, J., Passig, J., Radischat, C., Rabe, R., Reda, A., Rüger, C.,
956 Schwemer, T., Sippula, O., Stengel, B., Sklorz, M., Torvela, T., Weggler, B., and Zimmermann, R. 2016.
957 Aerosol emissions of a ship diesel engine operated with diesel fuel or heavy fuel oil. Env. Sci. Poll. Res. 1-
958 16. Doi: 10.1007/s11356-016-6724-z.

959 Stuut, J.-B., Zabel, M., Ratmeyer, V., Helmke, P., Schefuß, E., Lavik, G., and Schneider, R., 2005.
960 Provenance of present-day eolian dust collected off NW Africa. J. Geophys. Res. 110. Doi:
961 10.1029/2004JD005161.

962 Sunda, W.G., 2012. Feedback interactions between trace metal nutrients and phytoplankton in the
963 ocean. Frontiers Microbiol. 3. Doi: 10.3389/fmicb.2012.00204.

964 Thomson, R.E., Fine, I. V., 2003. Estimating Mixed Layer Depth from Oceanic Profile Data. J. Atmos.
965 Ocean. Technol. 20, 319–329. Doi:10.1175/1520-0426(2003)020<0319:EMLDFO>2.0.CO;2.

42

966 Torres-Padrón, M.E., Gelado-Caballero, M.D., Collado-Sánchez, C., Siruela-Matos, V.F., Cardona-
967 Castellano, P.J. and Hernández-Brito, J.J., 2002. Variability of dust inputs to the CANIGO zone. Deep Sea
968 Res. Pt II. 49, 3455-3464.

969 Venti, A., Kadko, D., Andersson, A.J., Langdon, C., Bates, N.R., 2012. A multi-tracer model approach to
970 estimate reef water residence times. Limnol. Oceanogr. Methods. 10, 1078–1095.
971 Doi:10.4319/lom.2012.10.1078.

972 Vitousek, P. M., Kennedy, M.J., Derry, L.A., and Chadwick, O.A., 1999. Weathering versus atmospheric
973 sources of strontium in ecosystems on young volcanic soils. Oecologia. 121, 255-259.

974 Winkler, R., Dietl, F., Frank, G., and Tschiersch, J. 1998. Temporal variation of [7]Be and ^{210}Pb size
975 distributions in ambient aerosol. Atmos. Environ. 32, 983–991. Doi:10.1016/S1352-2310(97)00333-6.

976 Xie, P., and Arkin, P.A., 2010. Global precipitation: A 17-year monthly analysis based on gauge
977 observations, satellite estimates, and numerical model outputs. Bull. Amer. Meteor. Soc. 78, 2539-2558.

978 Young, J. A., and Silker, W.B., 1980. Aerosol deposition velocities on the Pacific and Atlantic oceans
979 calculated from [7]Be measurements. Earth Plan. Sci.Lett. 50, 92-104.

980

981

982